IMPROVING LITHIUM-ION BATTERY POWER AND ENERGY DENSITIES USING NOVEL CATHODE ARCHITECTURES AND MATERIALS

BY

JONATHAN G. LANGE

THESIS

Submitted in partial fulfillment of the requirements
for the degree of Master of Science in Materials Science and Engineering
in the Graduate College of the
University of Illinois at Urbana-Champaign, 2012

Urbana, Illinois

Adviser:

Professor Paul V. Braun

ABSTRACT

Lithium-ion batteries are commonly used as energy storage devices in a variety of applications. The cathode architectures and materials have a large influence on the performance of lithium-ion batteries, namely power and energy densities. Three-dimensional bicontinuous cathode structures should help improve the charge and discharge rate performances, while maintaining a high energy capacity. By controlling the pore architectures of the bicontinuous cathode structures, we hope to manipulate the power densities to our advantage. Here we demonstrate synthesis of anisotropic silica colloids with precise control over particle dimensions. Using external AC electric fields and casting techniques, the anisotropic colloids were made into useful templates for cathode fabrication. Nickel electrodeposition through the anisotropic colloidal templates, with subsequent template etching, produced nickel current collectors with rod-shaped pore architectures. Thin-films of lithiated manganese dioxide were deposited onto the nickel current collectors, and the cathodes were analyzed.

New active materials in the three-dimensional bicontinuous cathodes should help to improve the overall energy density, without sacrificing structure-related power density. We demonstrate the ability to synthesize lithium manganese orthosilicate nanoparticles using a modified sol-gel route. Using this synthesis technique, a sol-gel dip-coating method on nickel foam is demonstrated and analyzed. These architectural and material fabrications demonstrated in this thesis provide new directions towards improving lithium-ion battery performance.

ACKNOWLEDGEMENTS

It is important to take this opportunity to express my gratitude to all those that have contributed to my graduate education. Foremost, I would like to sincerely thank my advisor, Professor Paul V. Braun, for his endless inspiration, support, and most importantly, his patience. His honest and positive criticisms have helped me recognize which aspects of science and engineering I thrive at. I truly admire his abundant intelligence and commitment to education. His influence will always remain with me.

Next, I would like to thank all the fellow Braun Group members, especially Dr. Jiung Cho, Dr. Huigang (Steven) Zhang, Kevin Arpin, and James Pikul for their insightful research discussions and experimental assistance. Kundan Chaudhary (from Dr. Jennifer Lewis's group) has been a significant contribution to this project, and collaborating with him has been enjoyable.

This research would not have been possible without the financial support of both the Frederick Seitz Materials Research Laboratory and the Beckman Institute for Advanced Science and Technology, here at the University of Illinois at Urbana-Champaign.

Finally, I would like to thank my parents and my sisters for all the support they have given me throughout my time at Illinois. Many times throughout this journey I was brought down by stress and I could always count on my parents to help me keep everything in perspective. I would not have come this far without my family's support.

TABLE OF CONTENTS

CHAPTER 1

INTRODUCTION

1.1 Lithium-ion Battery Technology

Batteries are used in almost every aspect of modern life. Everyday household items like flashlights, television remotes, and power drills require batteries. Even away from the house we depend on batteries to power our MP3 players, cell phones, and laptops. People with a pacemaker or other portable medical devices put significant trust in batteries. With the growing concerns of fossil fuel dependency and its environmental impacts, alternative energy has become a huge interest. However, alternative energy systems such as solar, wind, and hydro often require efficient batteries to store its energy. Hybrid or purely-electric vehicles need high-performance batteries in order to compete with existing gas-engine automobiles. These varieties of applications provide a massive demand for battery technology improvements.

Batteries are devices that convert chemical energy to electrical energy. Although primary batteries (non-rechargeable) have their uses, secondary batteries (rechargeable) appear to be more prevalent. Secondary batteries allow the reversible electrochemical reaction, where the electrical energy can convert back to chemical energy. This cyclability and reusability is desirable for most energy storage applications. Among the types of secondary batteries, lithium-ion batteries have gained particular interest because of their higher power densities, high capacity, slow self-discharge rate, low weight, high open circuit voltage, and negligible memory effect [1-3]. Despite their advantages, lithium-ion battery technology has room for improvement.

In order to develop better lithium-ion batteries, it is essential to recognize the basics of how a lithium-ion battery works. Within a lithium-ion battery, there are three basic parts:

cathode, electrolyte, and anode (figure 1.1). During battery discharge, lithium ions (Li^+) move from the anode to the cathode through the electrolyte. Simultaneously, free electrons (e^-) are produced in the anode, and then travel through the device (outside of the electrochemical cell) to the cathode. As electrons flow through the device, the lithium ions and electrons recombine in the cathode during this discharge. The electrolyte acts as a medium for ionic conduction and a barrier for electronic conduction. Whereas, the device and its pathway, acts as a medium for electronic conduction and a barrier for ionic conduction. This discharging mechanism uses the chemical energy as a driving force to produce electrical energy, which powers a device.

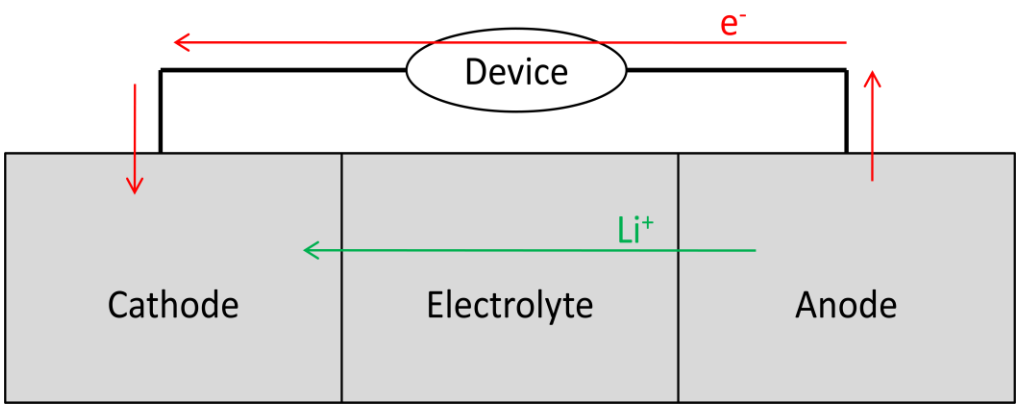

Figure 1.1. Schematic of the basic components of a lithium-ion battery cell during discharge.

To charge a lithium-ion battery, the device is replaced with a charger that applies an electric current and forces electrons to leave the cathode and move to the anode. Subsequently, lithium ions leave the cathode and intercalate into the anode to meet the electrons again. During this charging mechanism, electrical energy is used as a driving force to produce chemical energy. There are many things occurring within the battery during its usage. However, being able to quantify its performance is crucial for the advance of lithium-ion battery technology.

1.2 Performance Measures

Energy storage devices, such as lithium-ion batteries, are selected based upon the amount of energy they can store, as well as how fast they can be charged and discharged. These two performance characteristics are commonly known as energy density (specific energy) and power density (specific power). Depending on the application, these energy and power densities are either normalized to a weight (gravimetric) or a volume (volumetric). Batteries that must be designed to fit in a certain space will often be characterized by their volumetric energy and power densities. Whereas, when the battery weight is more critical, gravimetric energy and power densities may be useful. Ragone plots (figure 1.2) are charts used to compare the power and energy densities of various energy storage and conversion devices [4].

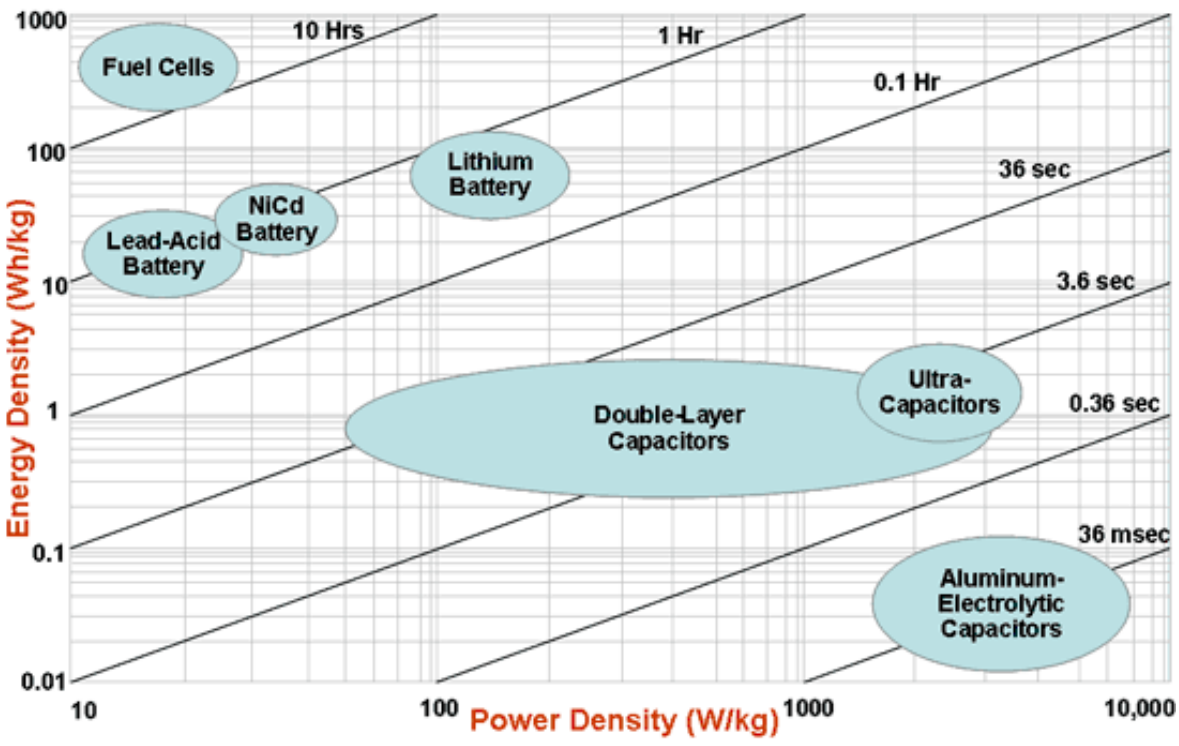

Figure 1.2. Ragone plot – comparison of performance of different energy storage devices. Figure adapted from "Meeting the Energy Needs of Future Warriors" [5].

Ragone charts typically plot energy density on the vertical axis and power density on the horizontal axis. The Ragone chart clearly illustrates that conventional capacitors have exceptionally high power densities, since they can quickly charge and discharge. However, capacitors also tend to have relatively lower energy densities and cannot store much energy. Typical batteries perform opposite to capacitors, as most batteries have comparatively higher energy densities, but lower power densities. This trade-off relationship between power density and energy density represents the challenge in lithium-ion battery design. The cathode of a lithium-ion battery is a large contributor to its overall performance. But by understanding the essential functions of the cathode, fundamental design changes can be made to improve both power density and energy density of lithium-ion batteries.

1.3 Basic Ideal Cathode Structure

It is important to understand what is occurring within the cathode so the basic design can be reevaluated. Lithium-ion battery cathodes must have two main components: an active cathode material and a current collector. Some common active cathode materials for lithium-ion intercalation-type batteries include lithium cobalt oxide ($LiCoO_2$), lithium iron phosphate ($LiFePO_4$), and lithium manganese dioxide ($LiMnO_2$), to name a few. The cathode current collector is the second main component of the cathode, and it serves as a pathway for electronic conduction. Some examples of typical cathode current collectors are porous carbon, nickel, aluminum, or copper. The active cathode material has one interface with the current collector (for electron conduction) and its second interface with the electrolyte (for lithium ion conduction). The active cathode material serves as a location for lithium ion and electron recombination during battery discharge. The same active material in the cathode is also the

location where lithium ion and electron separation occurs during battery charging. Understanding the basic structure of the active cathode material and the cathode current collector, can assist in explaining the typical trade-off between energy density and power density in lithium-ion batteries.

Lithium-ion cathodes with a relatively thick active cathode material (figure 1.3a) may prove to have higher energy densities since there is a higher density of active material. The more lithium ions that can be extracted, means more electrons can be extracted, and therefore more electrical energy can be generated. However, the trade-off for this thick film is its lower power density. This qualitative assumption can be made by understanding that the thickness of electrolytically active materials greatly affects the cycling rates [6]:

$$t \sim \frac{L^2}{D}$$

The time required for lithium ions to diffuse through the active cathode material (t), is related to the thickness (L) and the diffusivity (D) of the active cathode material. With an increase in thickness of active material, the time it takes for lithium to be extracted or intercalated will increase, yielding a lower power density. Therefore if the active cathode material is relatively thin (figure 1.3b), the power density should increase. Consequently, a thin film often means less active cathode material to extract energy; lower energy density. This thin-versus-thick active material explanation helps one to understand the trade-off between power density and energy density within lithium-ion batteries.

The thick film is attractive for its higher energy density, and the thin film is attractive for its higher power density. So if a thin film cathode is made in such a manner that it is manipulated to maximize its limited space, the amount of active material will increase, while maintaining a thin film (figure 1.3c). The basic ideal cathode structure will increase the power density while

preserving a high energy density. This ideal structure can also be termed as two-dimensional bicontinuous structure. However, real ideal cathodes will have similar bicontinuous architectures in three dimensions. It is also important to note that the active cathode material structure should have a high interfacial area with both the electrolyte and the current collector. An active cathode material that has a large interface with the electrolyte, but not with the current collector (figure 1.4d), will not have as high of power densities seen in the basic ideal structure. By creating cathodes with novel materials and better architectures, the trade-off of power density and energy density can be minimized.

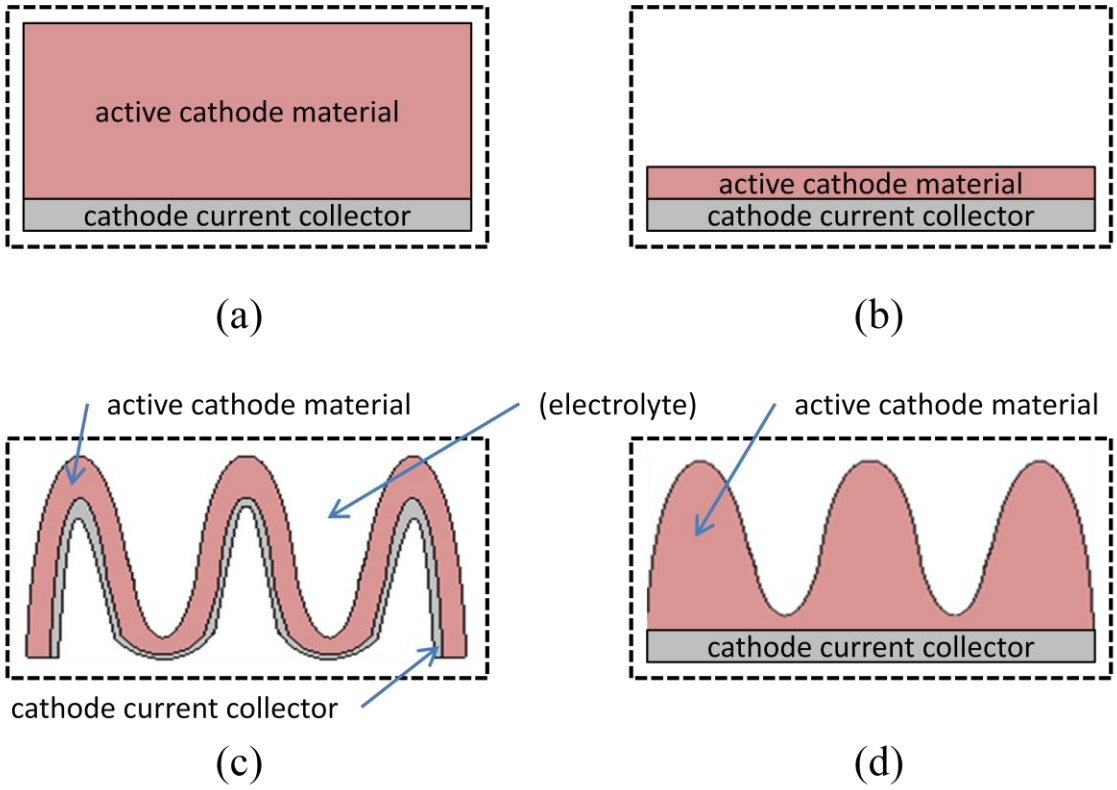

Figure 1.3. Schematic representation of basic cathode structural designs. (a) Thick active material – high energy density, low power density. (b) Thin active material – high power density, low energy density. (c) 2-Dimensional bicontinuous structure – high power density, high energy density, the "ideal" case. (d) High surface with electrolyte, still not enough of a thin film to have high power densities. Dashed-line box represents the same volume/weight constraints for each basic cathode.

CHAPTER 2

ANISOTROPIC COLLOIDAL TEMPLATES FOR BICONTINUOUS BATTERY ELECTRODES

2.1 Material Systems with Bicontinuous Structures

Bicontinuous structures provide the cathode's architectural requirements for high-performance. Bicontinuous is often described as a partitioning of volume that is produced by inscribing a continuous surface of positive genus [7]. Basically, it is a three-dimensional structure that has interpenetrating networks of high porosity. A bicontinuous metal scaffold may provide a feasible route for developing ideal cathode structures. The metal scaffold should be capable of serving as a cathode current collector with some mechanical rigidity. However, to provide superior performance, the cathode structures should have pore dimensions near micro and nanoscale sizes. These feature sizes will supply short ion and electron transport lengths, required for increasing lithium-ion cycling rates [8, 9]. Previous research involving bicontinuous structures has been done on a variety of material systems. These methods and systems could be adapted for developing ideal cathode structures.

A common method for creating bicontinuous structures is achieved using bijel templates. Bijels, bicontinuous interfacially jammed emulsion gels, are nonequilibrium structures formed by jamming of colloidal particles at the interface between two partially miscible fluids going through spinodal decomposition [10, 11]. Once the polymeric fluids are stabilized, the liquids can either be selectively polymerized, or both polymerized and selectively etched. This process yields a bicontinuous, soft organic polymer structure. By using an electroless deposition method [12, 13], a metallic coating can be deposited onto the bijel template. This bijel templating method provides a non-repeating bicontinuous structure that is a suitable architecture for a lithium-ion battery cathode (figure 2.1) [14].

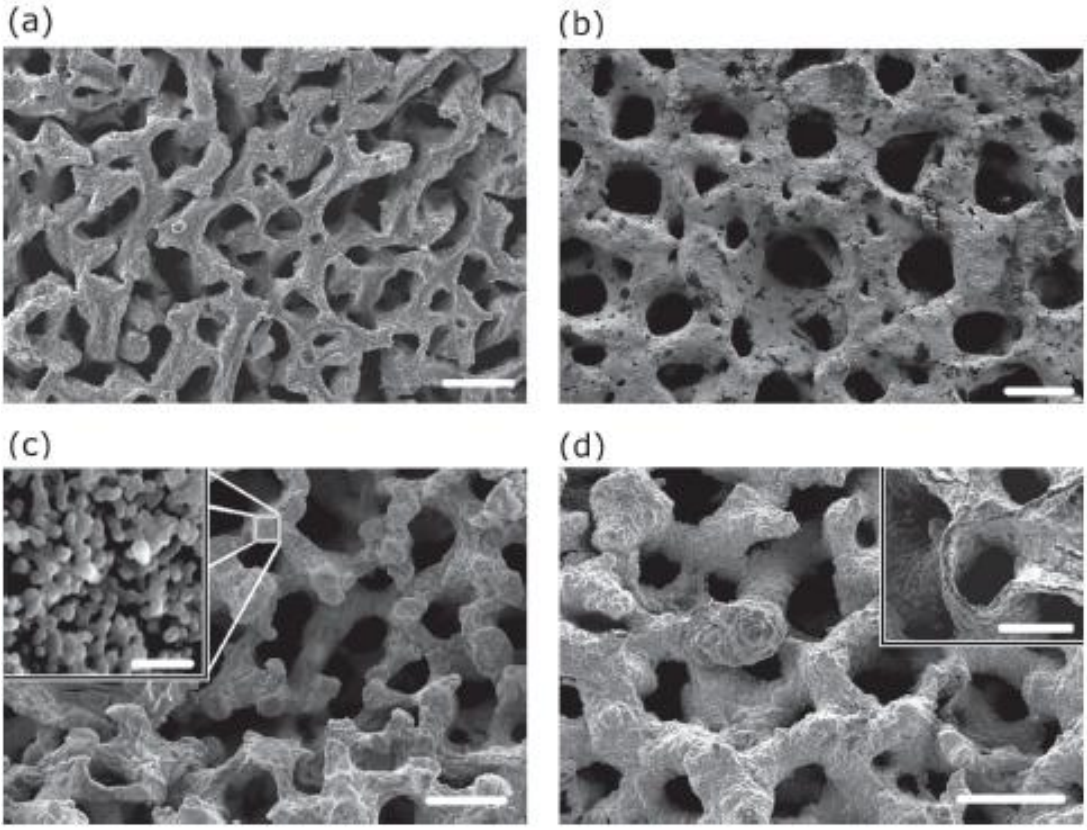

Figure 2.1. SEM images of bicontinuous materials using a polymerized bijel template. (a) Macroporous ceramic. (b) Copper-coated polymer. (c) Nickel network with hierarchical pore structure. (d) Spinodal nickel shell. Scale bars correspond to 50μm, insert scale bars (c): 500nm, and (d): 20μm. Adapted from "Bicontinuous Macroporous Materials from Bijel Templates" [14].

Another familiar bicontinuous material system consists of de-alloyed metals. This process involves creating a binary metallic alloy and then using selective dissolution to remove just one of the two metallic elements, yielding a bicontinuous metal [15]. This de-alloying has been observed by numerous binary systems including copper-gold [16], nickel-copper [17], magnesium-cadmium [18], and gold-silver [19], to name a few. Many of these investigations have also shown controllable adjustments of pore dimensions using acid immersions after de-alloying. Figure 2.2 shows a nanoporous gold structure after selective dissolution of silver [20]. The de-alloying method provides bicontinuous structures with a variety of metals, making it an attractive option for cathode current collector design.

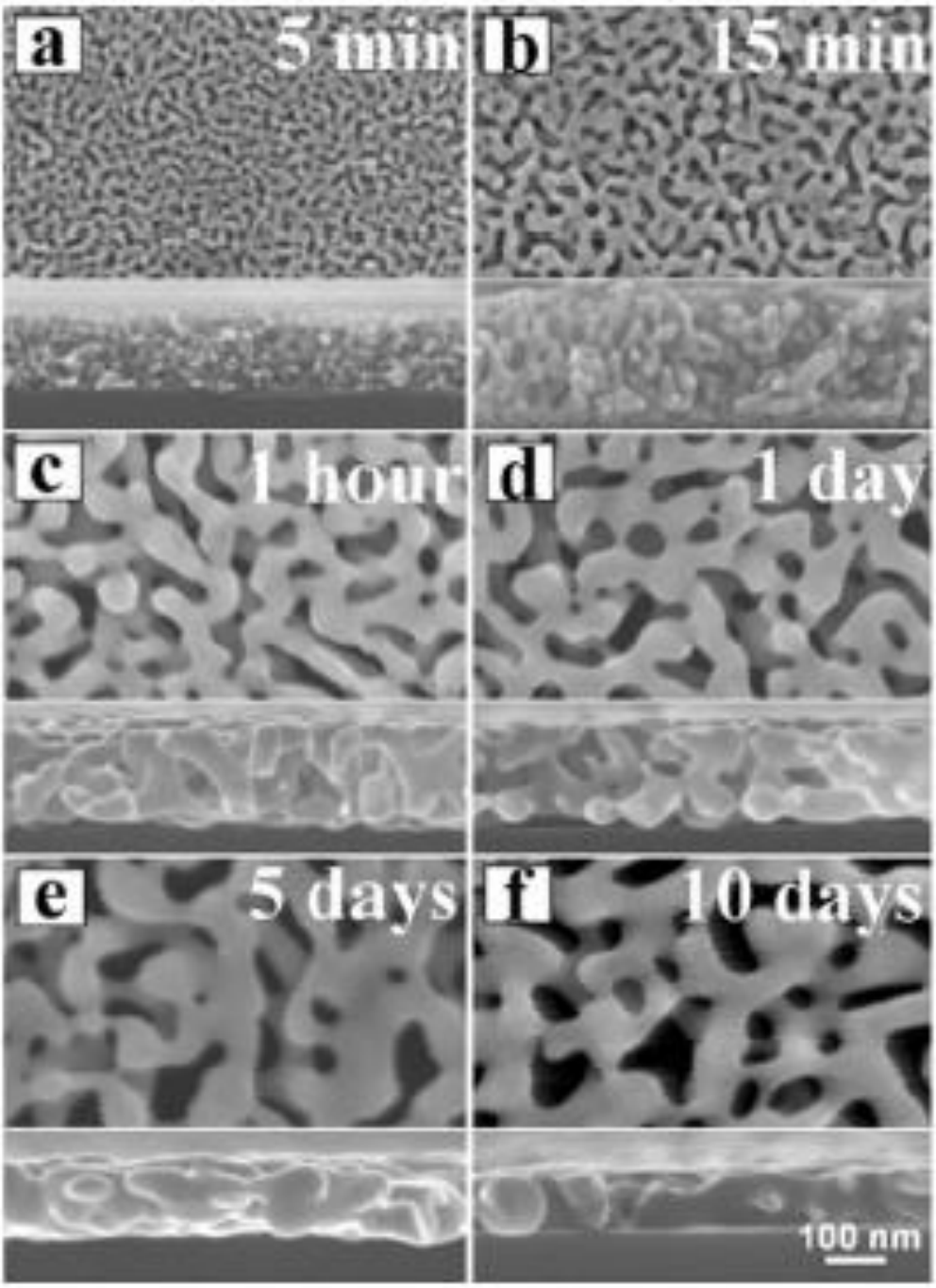

Figure 2.2. SEM images of nanoporous golf leaf samples. After de-alloying process, extended immersion in acid coarsens structure. Adapted from "Nanoporous Gold Leaf: 'Ancient Technology'/Advanced Material" [20].

Lithographic techniques using conventional phase-mask [21] and interference [22] lithography methods have been used to fabricate three-dimensional architectures that may be

suitable for lithium-ion cathodes. Photolithography uses light that travels through a photomask onto a polymer substrate that has light-sensitive chemicals (photoresist). The mask transfers geometric patterns onto the substrate, selectively exposing only parts of the photoresist. Three-dimensional structures can be made by interference of multiple waves (figure 2.3) or multiple exposures with different masks. The polymeric template can be used as a scaffold where metal can be deposited, making it plausible for current collector fabrication.

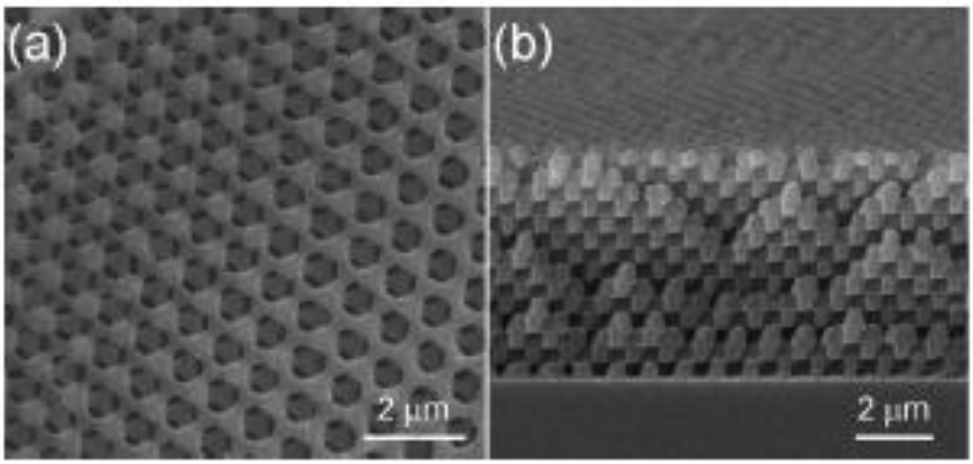

Figure 2.3. SEM images of polymer template with FCC-like lattice symmetry fabricated by holographic lithography. (a) Top-surface view. (b) Fracture cross-section. Adapted from "Fabrication of Three-Dimensional Photonic Crystals Using Multibeam Interference Lithography and Electrodeposition" [22].

Direct ink writing is a fabrication that utilizes an ink-deposition nozzle and a computer-controlled translation stage to create materials with controlled architectures [23]. Direct ink writing first requires an ink to be made. Concentrated colloidal, fugitive organic, and polyelectrolyte complexes are inks that can be used [24]. After directly writing the inks, the inks can solidify either by liquid-evaporation, temperature, gelation, or solvent-induced phase change. These directly written structures (figure 2.4) can either directly write metallic materials, or use

other materials that can be used as a starting template for subsequent metal deposition. Direct ink writing is an additional method that may be feasible for cathodic current collector fabrication.

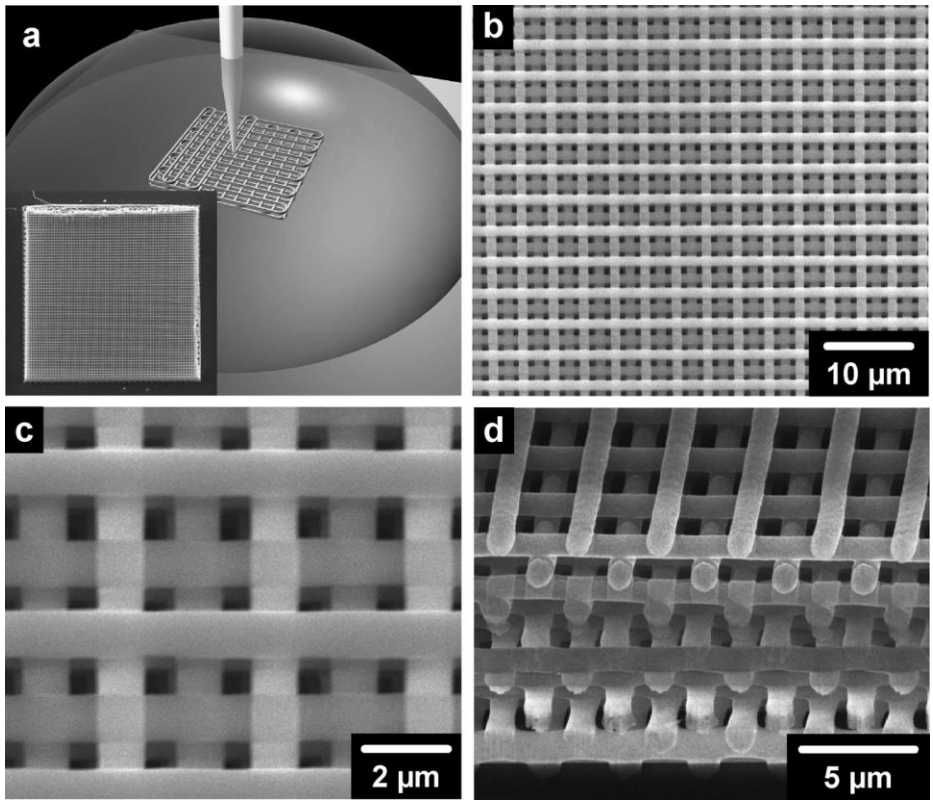

Figure 2.4. (a) Schematic illustration (inset is an SEM image of 250µm x 250µm woodpile structure. (b-d) SEM images of directly written structures. Figure adapted from "Direct-Write Assembly of Three-Dimensional Photonic Crystals: Conversion of Polymer Scaffolds to Silicon Hollow-Woodpile Structures" [24].

Inverse opals are another common material system with a bicontinuous structure. To create an inverse opal structure (figure 2.5), a three-dimensional colloidal crystal is first fabricated. A colloidal solution of particles, with particles ~0.1-2.5µm in diameter, is manipulated to assemble in close-packed arrangements. After drying, the colloidal crystal can be used as a spatial template for metal deposition. Chemical vapor deposition, atomic layer deposition, or electrodeposition of metals (or other materials) fills in the space between the

colloidal particles. After, the colloidal spatial template is removed, yielding highly porous, metallic architectures. The long-range ordering of the inverse opals is often attractive for photonic applications [25]. However, inverse opals are also a desirable option for cathode current collector structures.

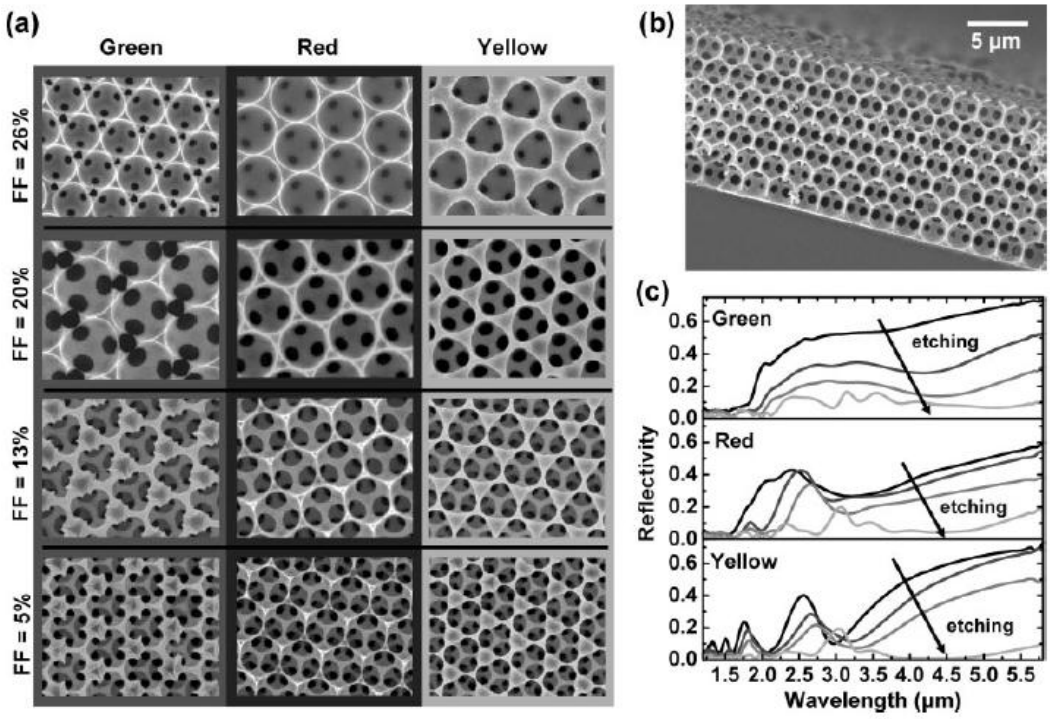

Figure 2.5. (a) SEM images of nickel inverse opal of different surface topologies and surface openness. (b) Cross-sectional SEM image of nickel inverse opal. (c) Reflectivity responses to nickel filling fraction. Adapted from "Filling Fraction Dependent Properties of Inverse Opal Metallic Photonic Crystals" [25].

2.2 Bicontinuous Electrodes using Close-Packed Nickel Inverse Opals

Recent research has been done using nickel inverse opals for developing bicontinuous cathode structures [26]. Inverse opal fabrication provides a simple, low cost, and reproducible method for creating advanced cathode current collectors. Zhang utilizes a fabrication approach (figure 2.6) that produces ideal architectures for cathode current collectors. A method to deposit

thin-film $LiMnO_2$ active material on the nickel scaffolds was also developed. These novel cathodes allow high charge and discharge rates while minimizing energy capacity loss.

2.2.1 Fabrication Approach

The fabrication of these cathodes first began with colloidal crystal growth on a conductive substrate. Evaporation-induced convective self-assembly is a well-known method for creating colloidal crystals [27]. After creating the opal template, nickel was electrodeposited on the conductive substrate. The opal template prevents nickel from depositing in the spaces taken up by the polystyrene colloidal particles. After electrodeposition, the polystyrene template was removed using an organic solvent. This nickel inverse opal could then be electropolished to reduce the amount of nickel (figure 2.7a). Only a small amount of nickel is needed to provide adequate electron conduction and mechanical stability for active material deposition. Manganese dioxide was electrodeposited on the nickel current collector (figure 2.7b). After, the manganese dioxide was lithiated (figure 2.7c) by immersing it in a hot lithium salt bath. This fabrication approach yields cathodes with a bicontinuous current collector coated with a thin-film active material.

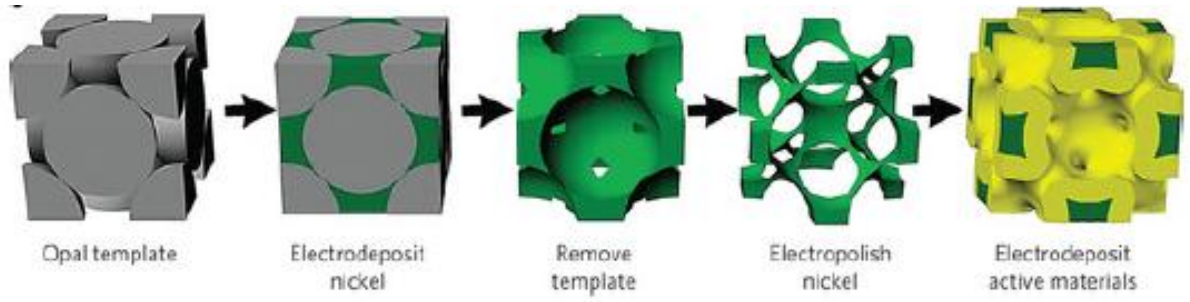

Figure 2.6. Schematic describing bicontinuous electrode fabrication process. Figure adapted from "Three-Dimensional Bicontinuous Ultrafast-Charge and –Discharge Bulk Battery Electrodes" [26].

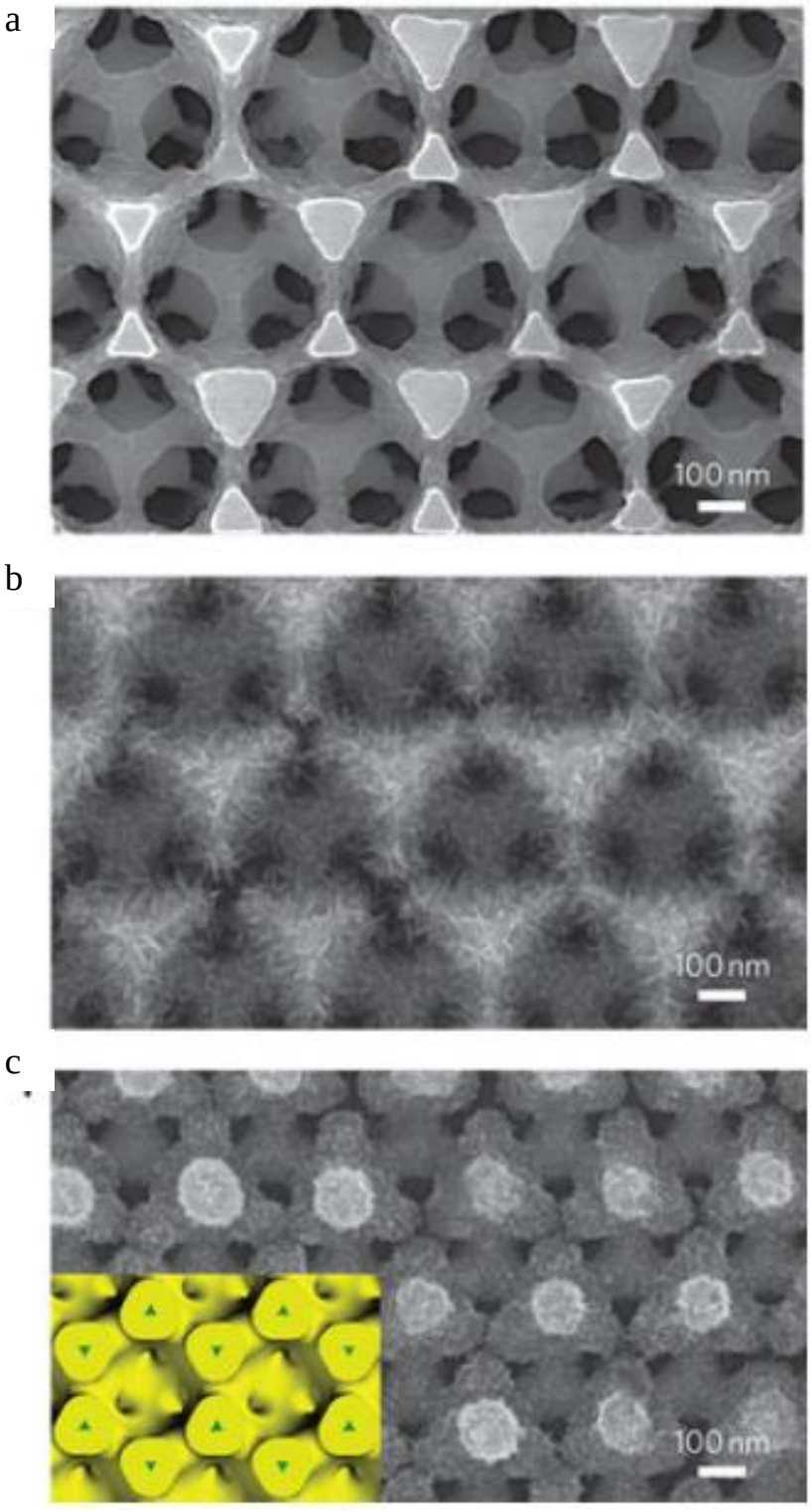

Figure 2.7. Cross-sectional SEM images of bicontinuous three-dimensional electrode during each step of preparation. (a) Nickel inverse opal after electropolishing. (b) MnO_2/nickel composite cathode. (c) Lithiated MnO_2/nickel composite cathode. Figure adapted from "Three-Dimensional Bicontinuous Ultrafast-Charge and –Discharge Bulk Battery Electrodes" [26].

2.2.2 $LiMnO_2$ Cathode Analysis

Zhang's $LiMnO_2$ bicontinuous cathode showed improved power densities while maintaining exceptional energy densities. The cathode was charged and discharged (figure 2.8) in a half-cell system. Lithium was used as a counter and reference electrode. The cathode was tested as several charge and discharge rates (C rates), where C is the number of discharges per hour. The cathode retained 76% of its capacity when discharged at 185C, and 38% when discharged at 1,114C. The cathodes tested had ~30nm of active $LiMnO_2$ material. However, it was also shown that thicker active materials (~150-200nm) have higher capacities, but sacrifice some cycling rate performance, which is an expected result.

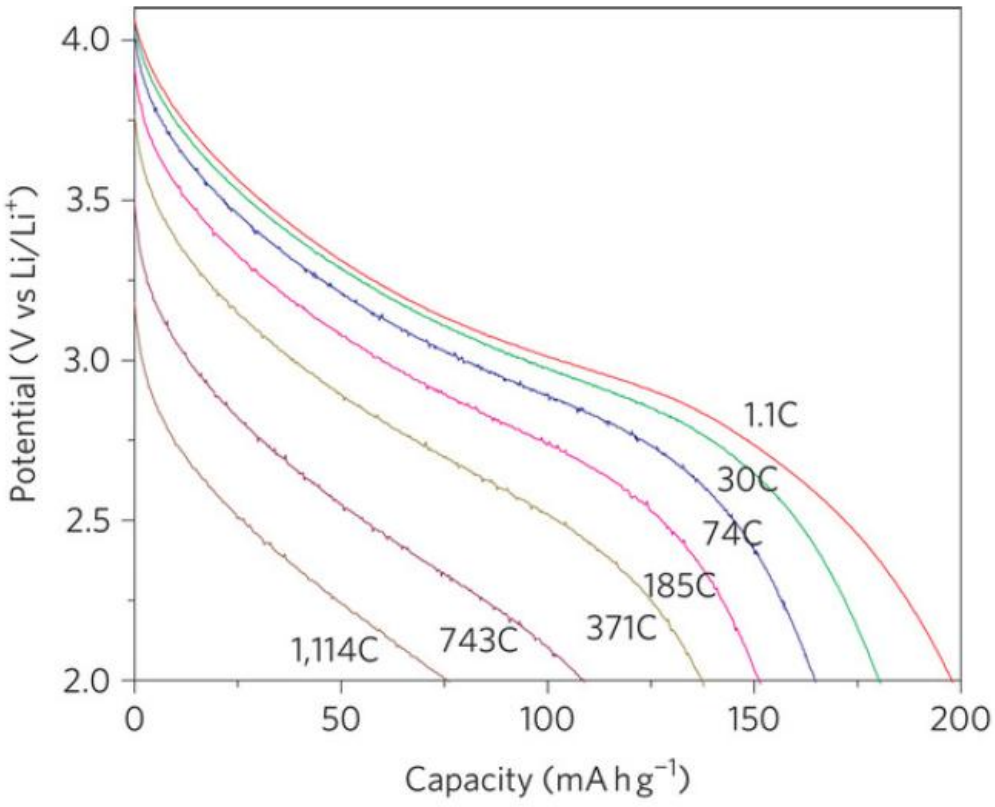

Figure 2.8. Lithiated MnO_2 cathode discharged at C-rates ranging from 1.1 to 1,114C. Adapted from "Three-Dimensional Bicontinuous Ultrafast-Charge and –Discharge Bulk Battery Electrodes" [26].

This $LiMnO_2$ bicontinuous cathode shows superb performance. The design minimizes the primary resistances within a cathode (figure 2.9). This fits within the regime of ideal cathode structures (figure 1.3c) described earlier. Using inverse spatial templates, these novel cathode current collector architectures can be made. The novel method of electrodepositing MnO_2 with subsequent lithiation provides a route for growing thin films of active cathode material onto a metallic current collector. Although this cathode system provides excellent performance, it may be desirable to alter its architecture. These close-packed opal templates produce structures with high tortuosity. This tortuosity may increase the resistance of lithium transport between the electrolyte and the active material, influencing its overall power density. Depending on the application, it may be desirable to have a similar cathode with different pore architectures.

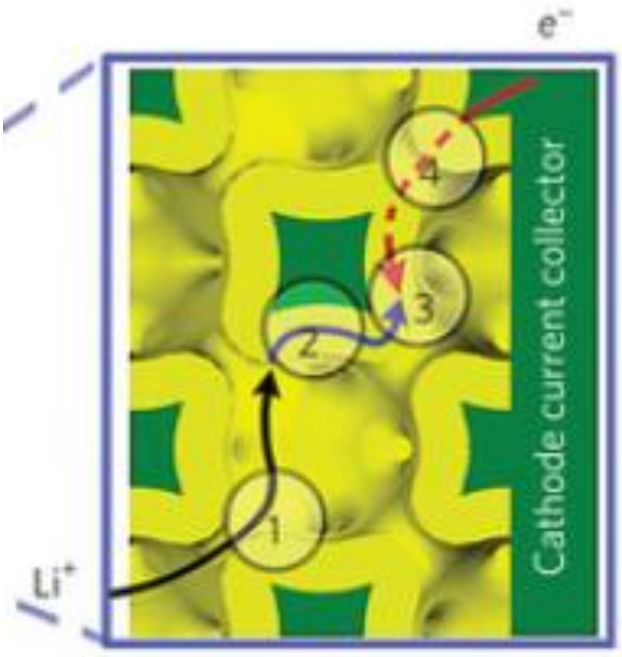

Figure 2.9. Schematic of the four primary resistances in a lithium-ion battery cathode. (1) Ion transport in the electrolyte. (2) Ion transport in the active cathode material. (3) Electrochemical reactions in the cathode. (4) Electron conduction in the active material and current collector. Figure adapted from "Three-Dimensional Bicontinuous Ultrafast-Charge and –Discharge Bulk Battery Electrodes" [26].

2.3 Current Collector Fabrication using SiO_2 Rod Templates

The aforementioned inverse opal fabrication provides an excellent starting ground for high-tech lithium-ion cathodes. For these systems, the shape of the pores heavily influences the charging and discharging rates. These pore shapes can be controlled by changing shape of the particles in the colloidal template. Rod-shaped colloidal particles (as opposed to spherical) may help to manipulate the performance of these bicontinuous cathodes.

2.3.1 SiO_2 Anisotropic Colloid Synthesis

Silicon dioxide (SiO_2), silica, anisotropic colloids have been previously developed. In order to adjust the cathode's pore architectures, it is crucial to be able to first synthesize these colloids and manipulate their dimensions. This section outlines the colloidal synthesis prepared by Kundan Chaudhary of Dr. Jennifer Lewis's group. The synthesis for the rodlike silica colloids was adapted from published procedures by Kuijk [28] and Zhang [29]. All glassware, including flasks, glass vials, and funnels were initially cleaned with detergents, water, and organic solvents. Next, the glassware was left in base bath for at least seven hours. Once removed from the base bath, the glassware was rinsed with copious amounts of Millipore water (resistivity at 18.2MΩ). The rinsed glassware was kept in a clean oven at 120-140°C until used.

The following section generally describes the procedure for synthesis of silica rods with dimensions of 1.7μm long and 225nm in diameter. However, it will be noted what needs to change in order to modify the dimensions and aspect ratios of the rods. For the first step of synthesis, 200mL of 1-pentanol (Sigma-Aldrich, #398268, ≥99%) was measured and poured into a 500mL round-bottom flask. Thirty grams of polyvinylpyrrolidone (PVP, Sigma-Aldrich, #PVP40) was weighed, and then added to the 500mL flask. An additional 100mL of 1-pentanol

was added to the flask. The flask was closed with an appropriate stopper and further sealed with parafilm. Following, the flask was placed in an ultrasonic bath (Fisher Scientific FS20H) for 3-4 hours. After gently shaking the flask, if the solution was clear and there were no polymer sediments at the bottom, the PVP was well dissolved in the 1-pentanol. Otherwise, sonication continued until the PVP was fully dissolved. Thirty milliliters of pure, 200 proof, ethanol (Decon Labs, #2701) was added to the flask. Next, 8.4mL of fresh Millipore water was also added. Subsequently, sodium citrate dihydrate (Fisher Scientific, #S279) was made into a 0.18M solution. Two milliliters of this solution was added to the flask, and the flask was gently shaken 15-20 times afterwards.

At this point, the mixture next needed to be filtered (figure 2.10). The mixture was poured from the flask into a clean beaker. Then the mixture was transferred into 60mL syringes and then attached to a syringe filter (Membrane Solutions, #SFPES025010S) with a pore size of 0.1μm. The syringe was set in a syringe pump (Harvard Apparatus) at a speed of 50mL/hr. The filtrate was collected in a clean flask. After, 6.75mL of ammonia (Acros Organics, #AC255210010, 25%) was added to the flask. Three milliliters of tetraethyl orthosilicate (TEOS, Acros Organics, #AC157811000, 98%) was added to the filtrate. The flask with the new filtrate solution was plugged with a stopper, and left in an environment that was stable enough to prevent any physical perturbations and fluctuations in temperatures away from ~20°C. After ~17hrs, the reaction was completed, and synthesized rods could next be harvested. As described by Kuijk, the length of this reaction time will control the rod length and roughly keep a fixed diameter around 225nm. If desired, the changing the reagent concentrations can also tune the dimensions of the rods [28]; however, this was not done for this project. Figure 2.11 is an image showing the monodispersity and rod size after filtration and synthesis.

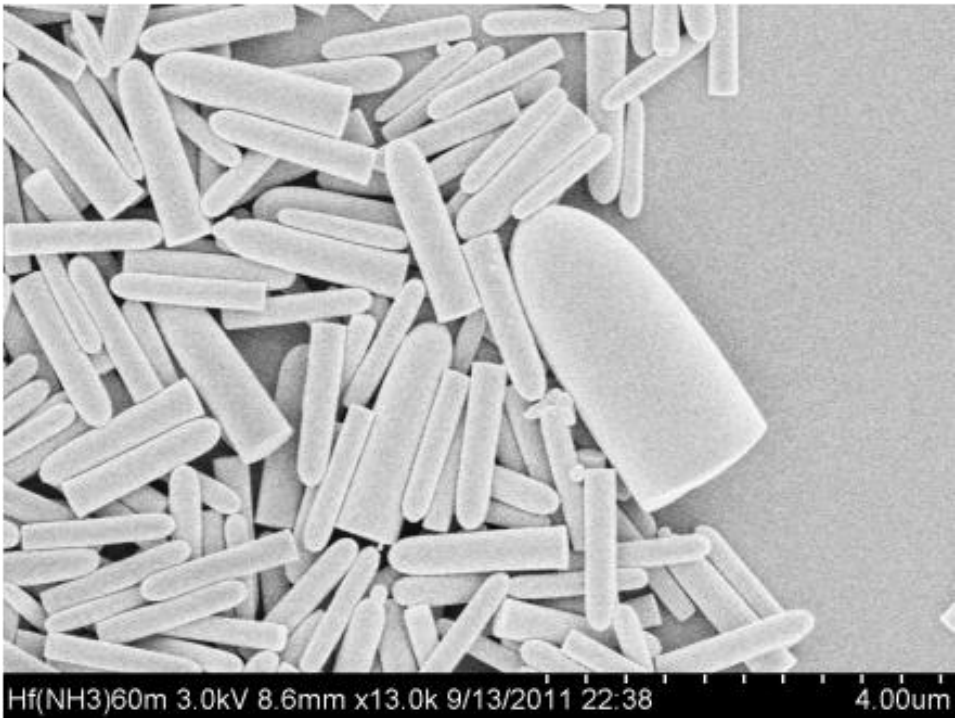

Figure 2.10. SEM image of synthesized SiO_2 anisotropic colloidal particles, unfiltered.

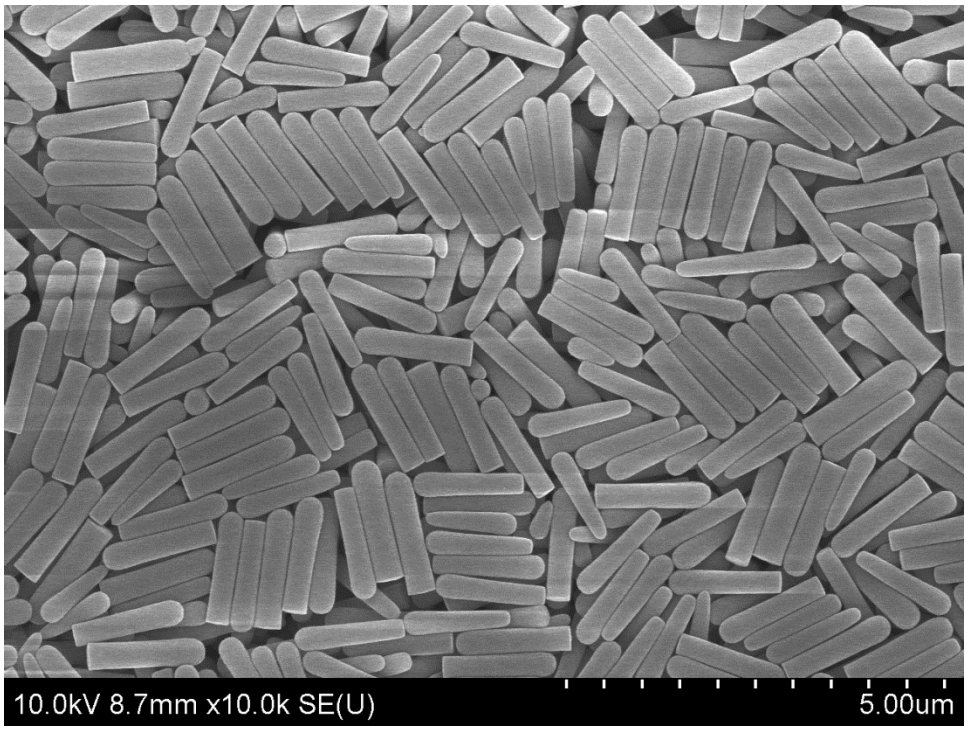

Figure 2.11 SEM image of synthesized SiO_2 anisotropic colloidal particles, filtered. Particle dimensions roughly 225nm in diameter and 1.7μm in length.

The newly formed rod colloid was transferred into 50mL centrifuge tubes. The samples were first centrifuged at 3000rpm for one hour. After, the supernatant was slowly poured out as waste. Thirty milliliters of ethanol was added to each tube. The samples were vortexed in their tubes until the rods were dispersed well. An additional 10 minutes in the ultrasonic bath proceeded. At this point, the rods have been completely dispersed in ethanol. Next, the samples were centrifuged at 2000rpm for 20 minutes, and supernatant was removed. Again, new ethanol was added, and sonicated until full dispersion. This centrifuge-sonication procedure was repeated an additional two times to thoroughly clean the rods. This step was repeated again, but instead of adding ethanol, Millipore water was added. After, the tubes were centrifuged for 15 minutes at 1500rpm, supernatant water removed, Millipore water added, and the sample sonicated until dispersion. This centrifuge-sonication step with water (previous sentence) was repeated until the supernatant maintained a pH of 7, or neutral, typically taking 3-6 repetitions. At this point the rods were either prepared in their proper concentrations (skip the next paragraph) or grown to make larger silica rods (described next).

To increase the dimensions of the rods (not just the length), the rods were first dispersed in 50mL of ethanol, then poured into a clean 500mL flask. With a magnetic stir bar stirring, 6mL of ammonia (25% in water) was added and then 5mL of Millipore water. Subsequently, 0.5mL of TEOS was added to the flask. After six hours of the reaction, 0.12mL of Millipore water was added along with another 0.5mL of TEOS for the second layer of silica. After this second silica layer, the growth was able to be continued by more Millipore water and TEOS (same amounts as aforementioned) additions every three hours. To create a rod with a diameter of ~1μm, it approximately took 19 additions. Figure 2.12 shows a sample of rods that were grown using this

process. Once the desired particle size was reached, the particles were washed in ethanol and water, as described previously.

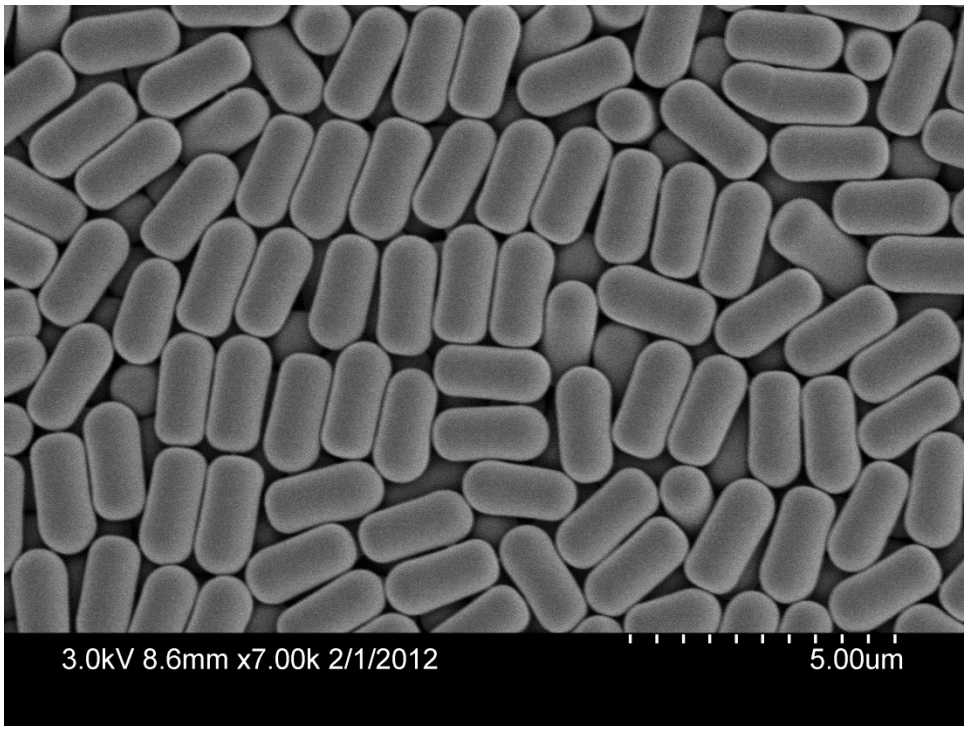

Figure 2.12. SEM image of SiO_2 anisotropic colloidal particles that were given 19 TEOS additions after synthesis of seed particles (225nm diameter and 1.7μm length). Particle dimensions roughly 2.5μm in length and 1nm in diameter.

After the rods were grown to the desired size and washed thoroughly, they were stored in ethanol in a clean glass vial. The glass vial was wrapped by filter paper on a hot plate to completely evaporate the ethanol. The filter paper was sealed with parafilm, and the vial left uncapped. After drying, some rods were extracted and weighed. Once the volume of the rods was determined, Millipore water was added to the rods to create a desired solution concentration. Most rod solutions used were typically 1-5vol% SiO_2. These solutions were sonicated for ~2hrs before being used the rods as structural templates for the current collector.

To create the colloidal templates with different pore architectures, it is required to synthesize colloids with anisotropic shapes. We have shown that we can synthesize these rods with high monodispersity. This synthesis procedure allows one to manipulate both diameter and length dimensions, giving great control over the particle sizes and aspect ratios. In turn, this should allow us to manipulate pore dimensions. Now that a synthesis for template particles has been established, the next step is to assemble the colloids into favorable templates.

2.3.2 SiO_2 Rod Assembly Techniques

After synthesizing the silica anisotropic colloids, the next step is to assemble the particles in useful templates for bicontinuous electrode fabrication. There are three basic orientations that the SiO_2 rods can directionally orient. Rods can be aligned perpendicular to the substrate (figure 2.13a). This structure may provide high power densities since the flow of lithium ions will have a direct away from the substrate. Rods can be horizontally oriented (figure 2.13b). This orientation may be favorable to interdigitated microbatteries, where the direction of lithium transport is mostly parallel to the substrate's face. The final orientation is random alignment (figure 2.13c). The work outlined in this section was done in collaboration with Kundan Chaudhary of Dr. Jennifer Lewis's group.

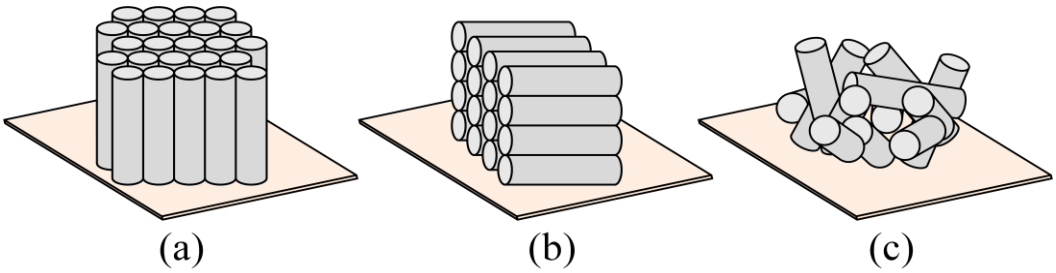

Figure 2.13. Schematic of possible orientations of SiO_2 rods. (a) Vertically aligned. (b) Horizontally aligned. (c) Randomly aligned.

Previous work has shown that charged colloidal particles, including silicon dioxide, will reconfigure their molecular electron charge distribution in the presence of an external electric field [30]. It is also plausible that applied electric fields can induce orientation parallel to the external fields [31, 32]. This technique of electric field-induced particle-alignment was utilized for vertical and horizontal orientation of the SiO_2 anisotropic colloids. For the vertical assembly, approximately ~30μL of ~2-3vol% SiO_2, in water, colloid was placed on an indium tin oxide coated glass slide (ITO, Sigma-Aldrich, #703192, 8-12Ω/sq). The ITO provided conductivity required for the applied electric field. Double-sided scotch tape was placed on the surface of each side ITO substrate. After, another ITO substrate was placed on top of the tape with the ITO coating facing towards the colloid. The tape acted as a ~76μm insulating spacer, preventing shorting between the ITO electrodes. The tape was also thin enough to allow an effective field to induce orientation within the colloid (figure 2.14). The two ITO electrodes were connected to an electric function generator (Agilent). Since the ITO coated glass was transparent, we were able to use oil immersion microscopy (Olympus, 60X magnification) to monitor alignment of the rods. By tuning the frequency of the AC-electric field around ~100kHz and the peak-to-peak voltages near ~5V, we were able to vertically align the silica rods (figures 2.15 and 2.16).

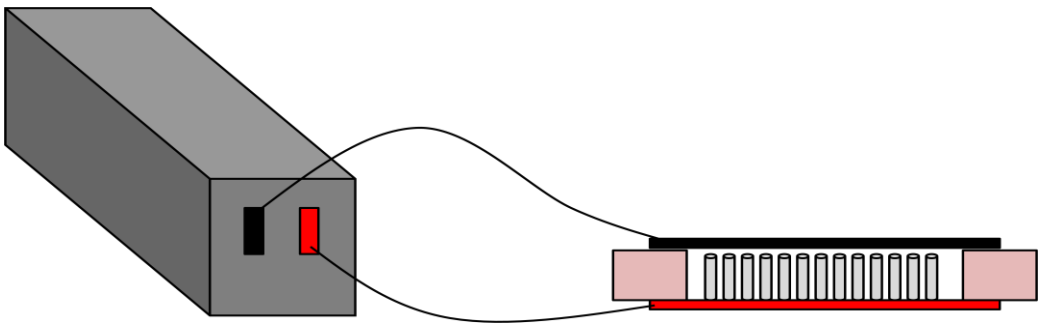

Figure 2.14. Schematic of vertical alignment assembly method. Electric field applied from a function generator to top and bottom electrodes. Spacer used between electrodes.

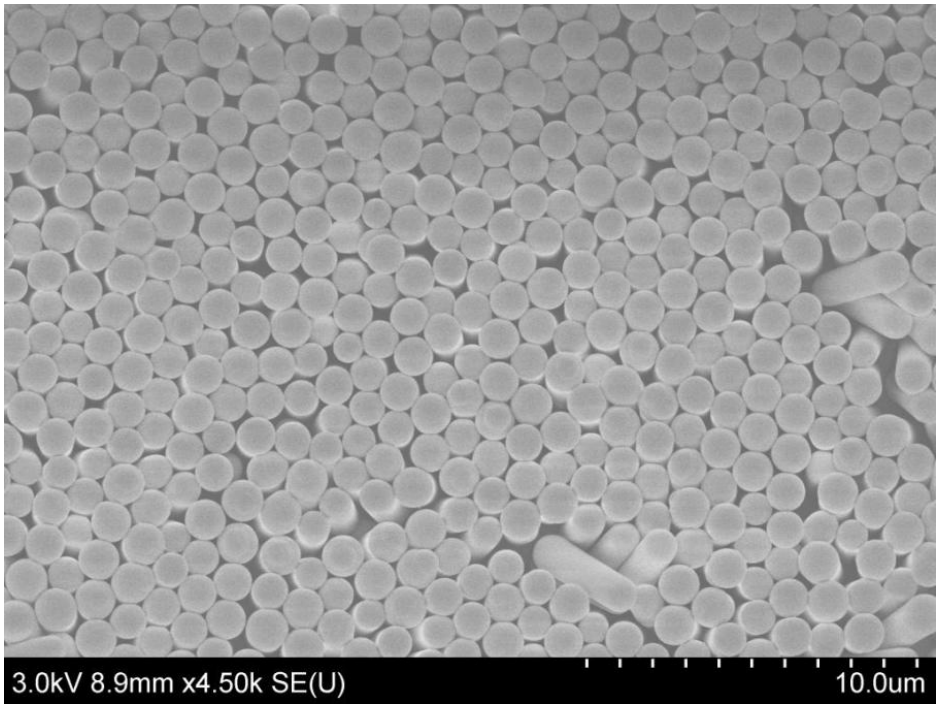

Figure 2.15. SEM top-view image of vertically aligned SiO_2 rods.

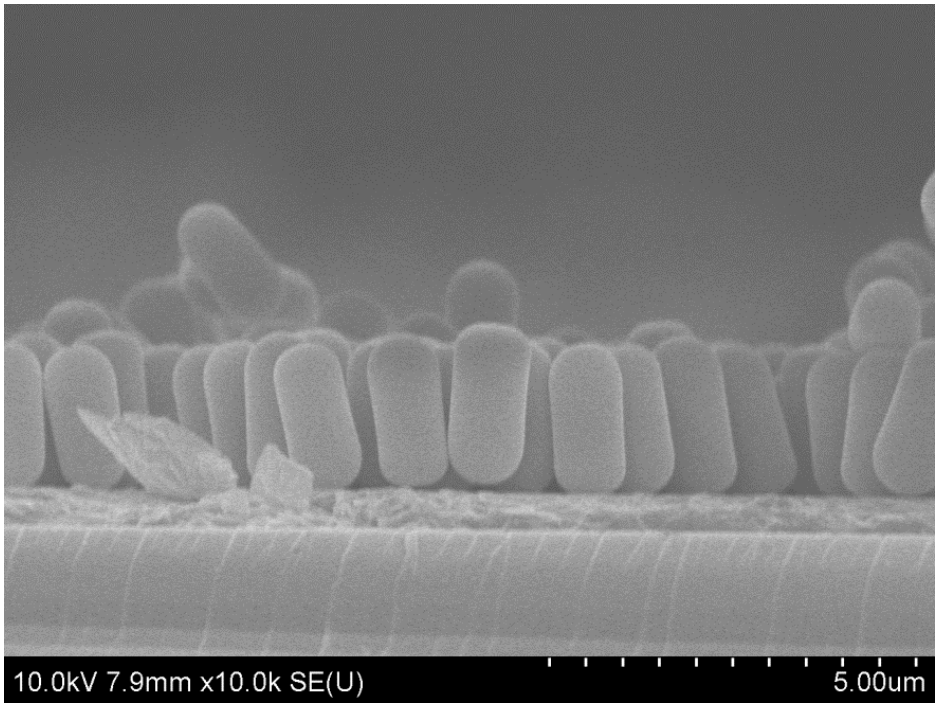

Figure 2.16. SEM cross-sectional image of vertically aligned SiO_2 rods.

Horizontal assembly was achieved using a similar technique as the vertical assembly. Two conductive pathways, either made of copper tape (3M, #1181-1/4~X18YD) or evaporated gold, were put onto an ITO glass cover slip. These two electrodes were placed ~100-500μm apart. After, ~20μL of ~2-3vol% SiO_2, in water, colloid was placed on the prepared substrate so that at least some of the colloid was placed between the electrodes (figure 2.17). Using oil immersion microscopy, from below the substrate, it was possible to fine tune the parameters for horizontal alignment. Although the electric field required depends on a variety of conditions such as rod size, electrode spacing, and particle concentration, the frequencies required for horizontal alignment (figure 2.17) were around ~100kHz with ~5V peak-to-peak voltages.

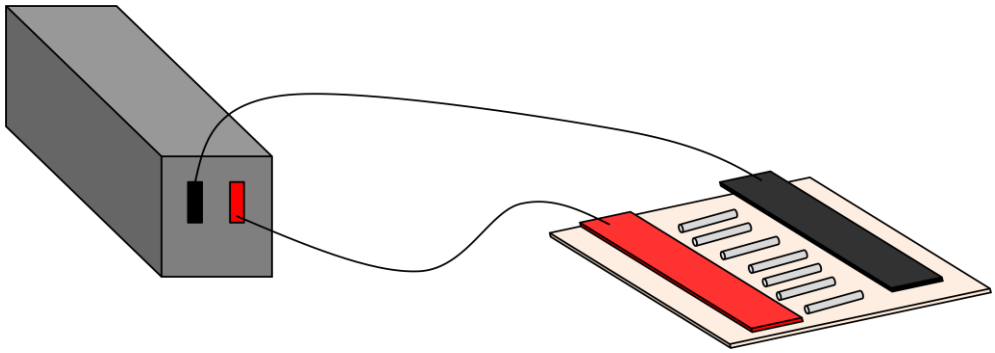

Figure 2.17. Schematic of horizontal alignment assembly method. Electric field applied from a function generator to two electrodes spaced on a substrate.

For both vertical assembly and horizontal assembly, an electric field is required to align the particles. The SiO_2 particles first begin to align while in the water. However, to prepare the templates, the solution is required to dry leaving just the particles behind. For each of these aligned assemblies, the electric field is applied and held for ~4-10 hours until dried. A small glassware dish placed over the substrate helped to prevent rapid evaporation.

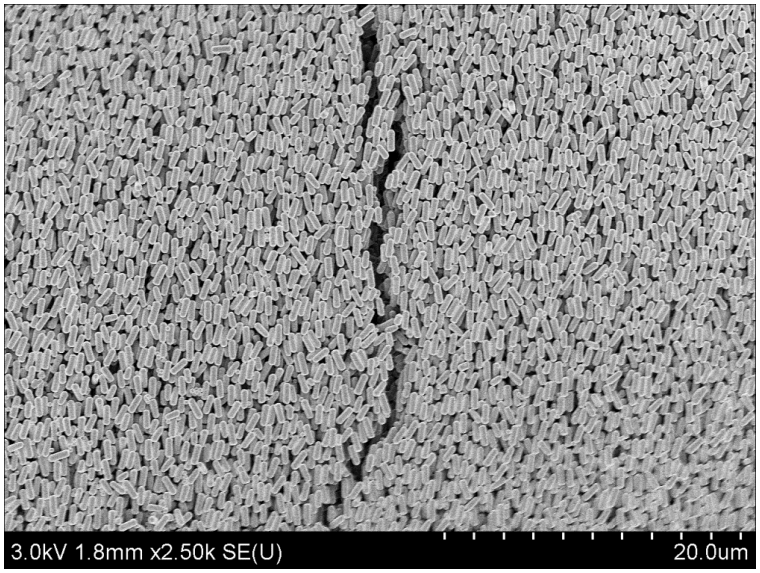

Figure 2.18. SEM top-view image of horizontally aligned SiO_2 rods.

Random alignment of the anisotropic colloids was the simplest procedure of the three template assemblies. Tungsten foil substrates (Sigma-Aldrich, #357197, ≥99.9%) were cut into ~1 inch x ~0.5 inch pieces. Roughly 30μL of 1-2vol% SiO_2 colloid, in water, was cast onto the tungsten substrates. The substrates were placed onto a hot plate set at an intermediate setting. After ~10-20 minutes, the samples were dried (figure 2.19).

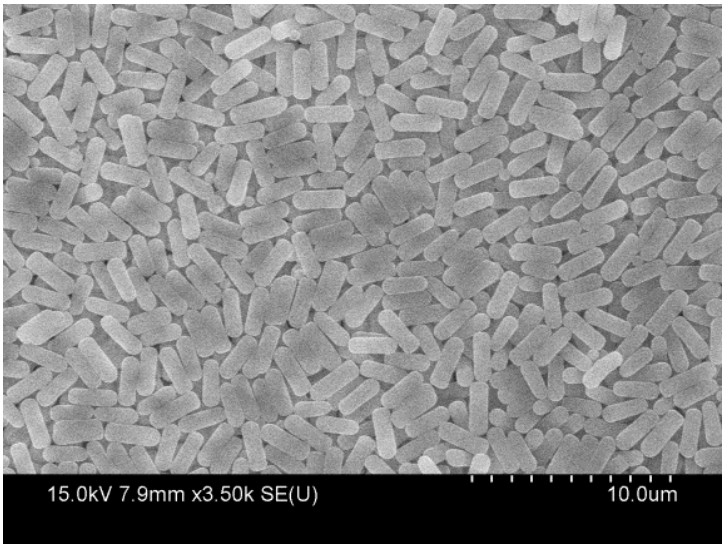

Figure 2.19. SEM top-view of randomly aligned (no directional orientation) SiO_2 rods.

After drying the assembled templates, the samples were sintered in a horizontal tube furnace at ~500°C in air for ~3 hours. ITO coated glass slides were used as conductive substrates for the aligned samples. The ITO's transparency allowed the use of microscopy during alignment to fine tune the parameters for effective control over the orientation. However, tungsten substrates have replaced the ITO glass slides to allow etching of the SiO_2 templates (described in the next section). To test the cathodes, it is required that the colloidal templates are a practical size. 5mm by 5mm template areas are the minimum size required for electrochemical testability. Adjusting the colloidal concentrations and drying conditions allows us to control the template thickness to be ~20-25μm. This range of template thickness is thin enough to prevent cracking during sintering and it is thick enough to provide an effective influence from its bicontinuous structure. Other methods to hold the template structure together during drying are being investigated. These methods include ultraviolet curing of polymers in the colloid or super-critical drying. Other assembly methods are also being researched, including convective self-assembly and direct writing of anisotropic colloids. However, the assembly methods here prove that we can manipulate the particles to orient vertically, horizontally and randomly, the three basic possibilities.

2.3.3 Nickel Infiltration and Template Removal

After the anisotropic colloidal template is developed, the next step in the cathode fabrication was to deposit a current collector material. The colloidal templates were deposited on conductive substrates to allow electrodeposition through a bottom-up growth technique. Commercial nickel electrodeposition solution (nickel sulfamate, Technic Inc., #030179) was poured into a 60mL glass container. Using a two electrode system, the colloidal template

substrate was connected to an alligator clip, further connected to a potentiostat (BioLogic) as the working electrode. A platinum foil strip (Sigma-Aldrich, #267260, 99.99%) was cleaned in 0.1M HCl with a subsequent water rinse. This step cleans any debris off the platinum between electrodepositions. The platinum strip was used as both the counter and reference electrode. At this point, the potentiostat was programmed to apply a cathodic constant current. The electrode size influences the amount of current required for nickel electrodeposition. For ~1cm^2 substrates, -1mA was required for roughly ~2-4 hours to deposit nickel to a thickness ~20μm. The thickness of the nickel was adjusted by controlling the electrodeposition time. Figure 2.20 shows the nickel electrodepositing through a randomly oriented template. We use a bottom-up approach on metal growth, permitting more room for error in electrodeposition parameters. Large cracks (~30μm) that formed from template drying in the previous process, do not pose much of a problem. Those cracks fill with nickel, and as long as there were not high densities of cracks, there was still a high density of structured area (figure 2.21).

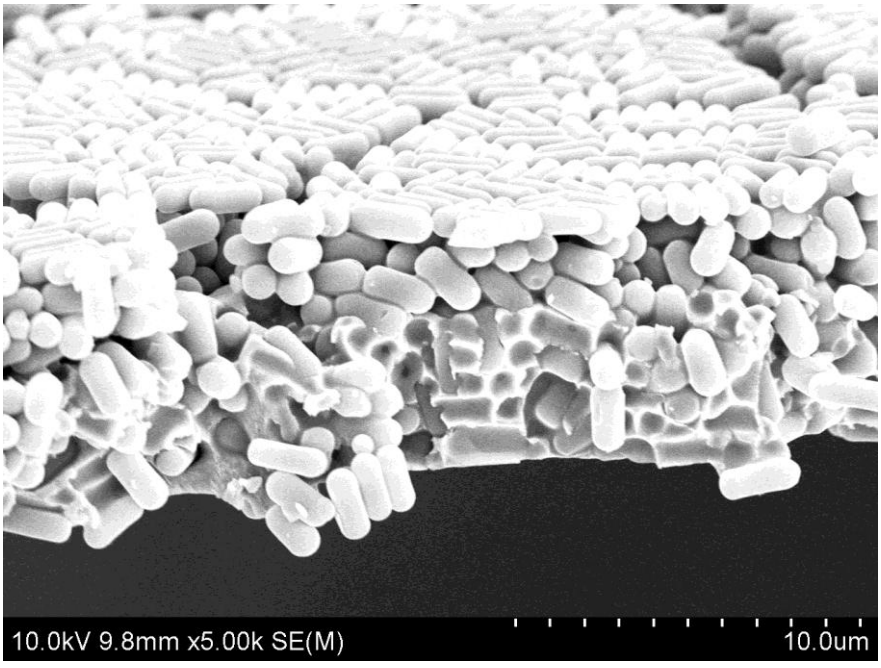

Figure 2.20. SEM image of ~6μm nickel electrodeposited within ~9μm thick randomly-oriented template.

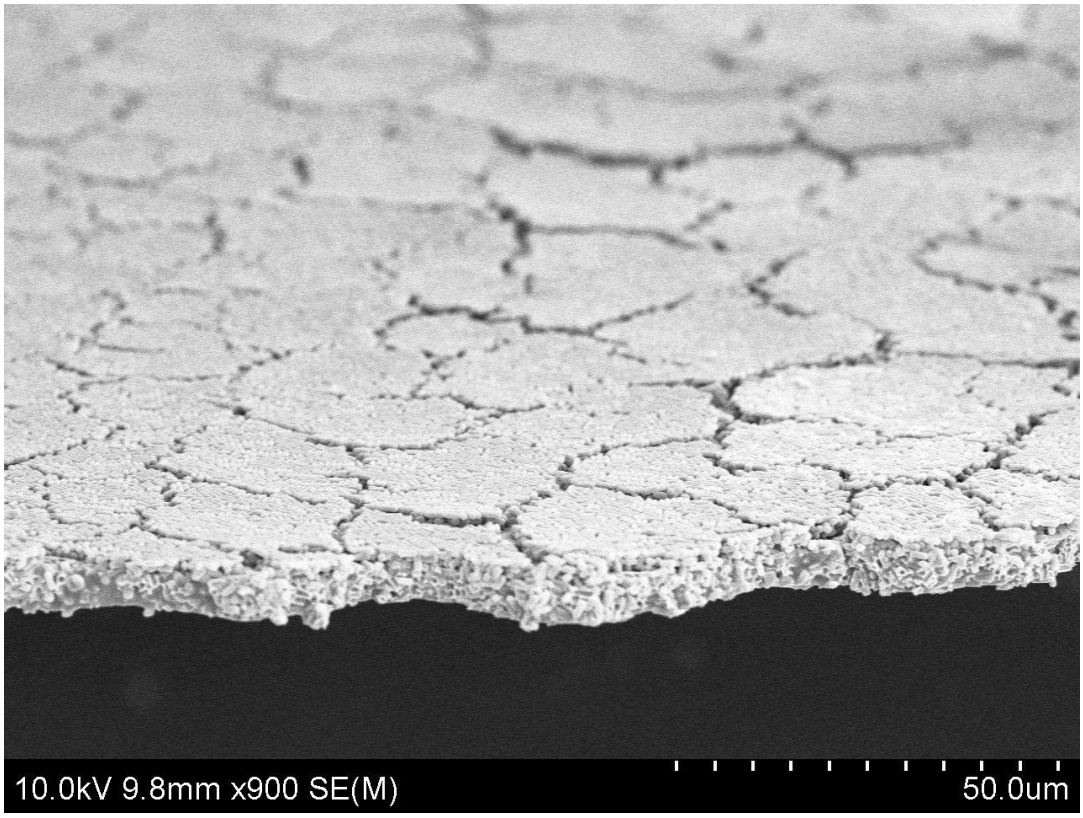

Figure 2.21. SEM image of a large, randomly-oriented template with nickel electrodeposited partially through the substrate.

After, infilling the spaces between the anisotropic colloidal particles in the template, the next step is to remove the template to yield the highly porous nickel architectures. Zhang's polystyrene templates were removed using tetrahydrofuran. Here, ethanoic hydrofluoric (HF) acid was required to etch the SiO_2 templates. 5% HF ethanoic solution was created by mixing 4mL HF buffer solution (Sigma-Aldrich, #695068, 48%), 18mL Millipore water, and 18mL ethanol in a 60mL Nalgene container. After mixing, the samples were placed in this ethanoic HF for ~10-15 minutes until the SiO_2 was completely etched. Subsequent washing with water removes the HF and SiO_2 residue. The silica template removal was successful for a variety of pore sizes within the nickel current collector (figures 2.22, 2.23, and 2.24).

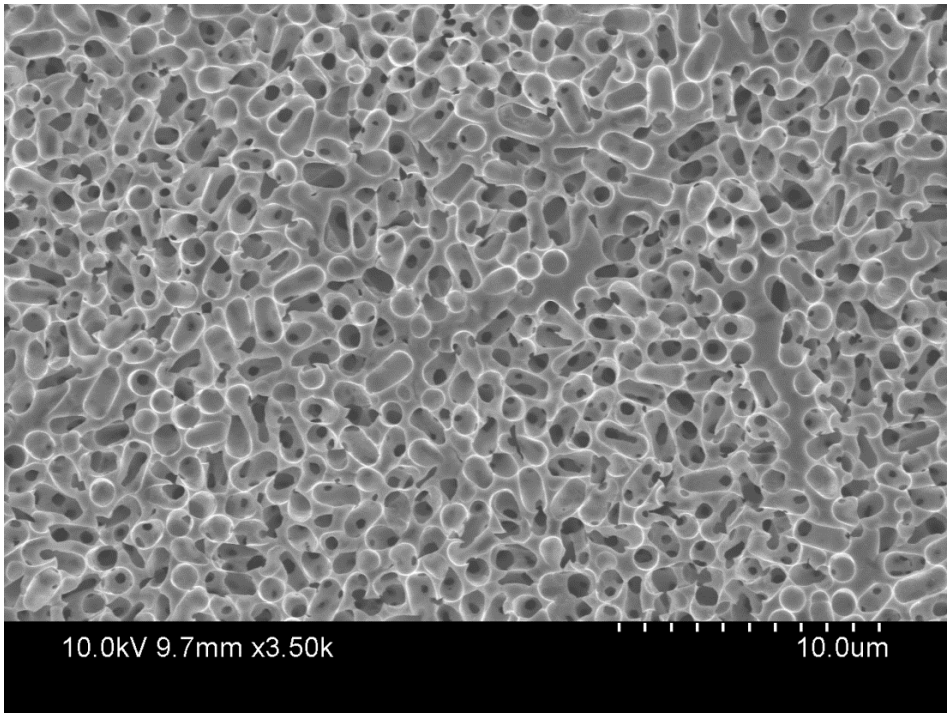

Figure 2.22. SEM top-view of etched nickel current collector. Randomly-oriented pore sizes are ~1μm diameter by ~2.5μm length.

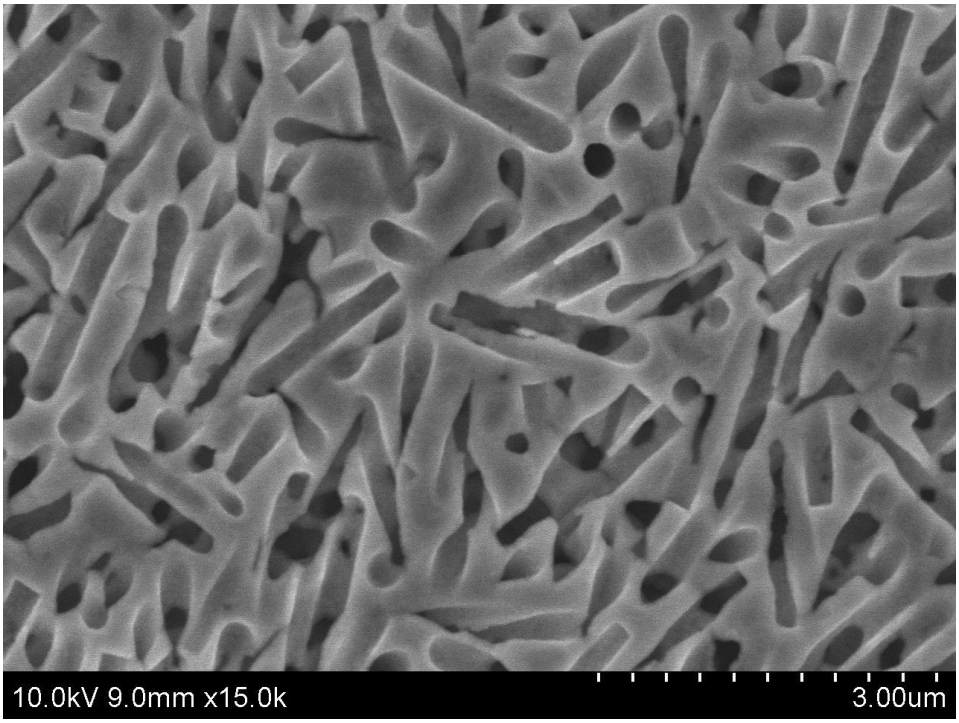

Figure 2.23. SEM top-view of etched nickel current collector. Randomly-oriented pore sizes are ~1.8μm length by ~250nm diameter.

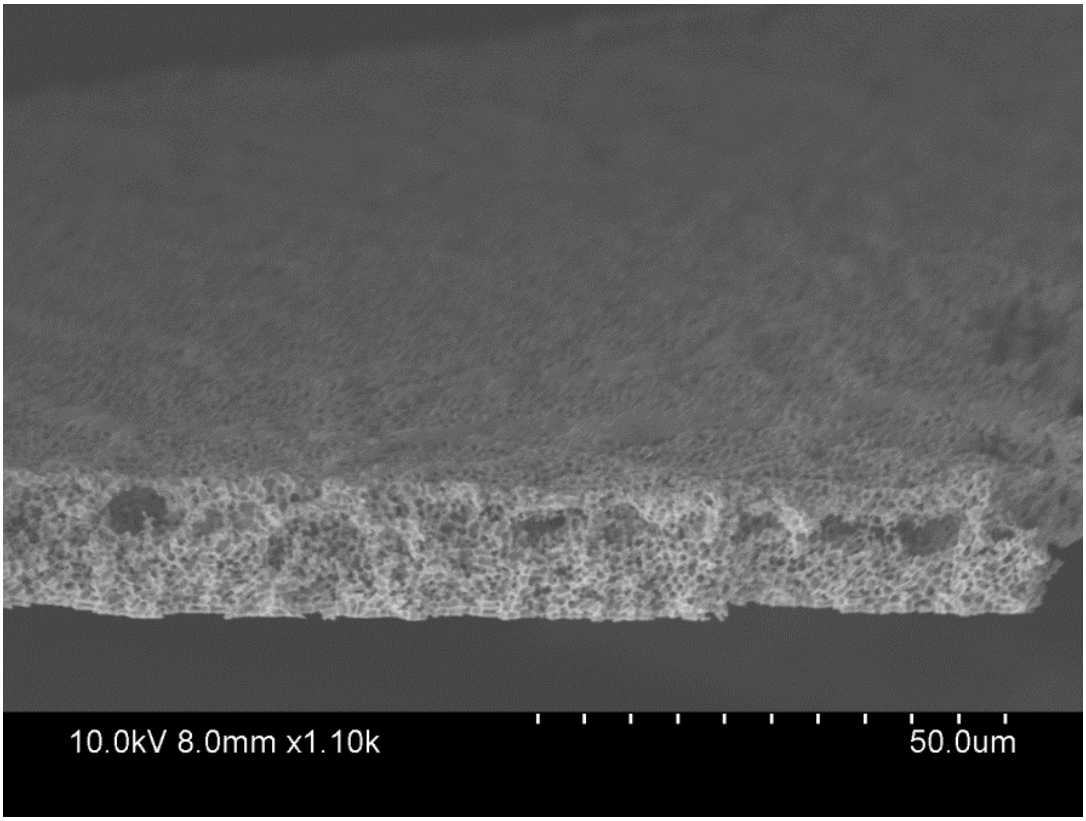

Figure 2.24. SEM image of ~18μm thick etched nickel current collector with randomly-aligned pores.

In this section, we have shown that we can synthesize rods with high monodispersity. Our synthesis allows adjustable variables that we can use to manipulate the dimensions of the SiO_2 rods. These anisotropic particles can be assembled in several orientations using external electric fields and slurry casting techniques. We have also shown that we can use these anisotropic colloidal assemblies to create spatial templates during nickel electrodeposition. After infilling the spaces with nickel, it was shown that we can etch these particles to produce highly porous nickel architectures. These architectures allow us to fabricate cathode current collectors with different pore shapes and dimensions.

2.4 Bicontinuous $LiMnO_2$ Cathode with Rod-Shaped Pores

We have shown that nickel current collectors can be fabricated using anisotropic colloidal templates. However, these current collectors are only half of the cathode. To turn these structures into a working cathode, an active cathode material must be incorporated. Using similar techniques as Zhang [26], thin films of lithiated MnO_2 are coated on the anisotropic bicontinuous architectures.

2.4.1 MnO_2 Deposition and Lithiation

The first step in developing the thin film lithiated MnO_2 films is electrodeposition of manganese oxide-hydroxide (MnOOH). Manganese oxide-hydroxide plating solution was synthesized. First, 50mL of Millipore water was put into a 60mL Nalgene container. After, 1.22g of manganese (II) acetate tetrahydrate ($MnAc_2$, Sigma-Aldrich, #63537, ≥99.9%) and 0.7g sodium sulfate (Na_2SO_4, Acros Organics, #21875, 99+%) were thoroughly mixed into water. Adding ~0.5mL of ethanol to the solution helped wet the surface of the nickel current collectors. To plate the nickel current collectors with the MnOOH, a two electrode system was used. The nickel samples were clamped to an alligator clip and connected to the potentiostat as the working electrode. Cleaned platinum was used as the counter and reference electrode, as it was in nickel electrodeposition. In this plating method, the entire nickel sample is conductive and the plating procedure requires more careful attention. Anodic pulses of 2.0mA for 1 second on and 0.0mA for 10 seconds off were applied for ~400 cycles (substrate size ~1cm^2, ~18μm thick). Without this cycling procedure, MnOOH will only coat near the surface of the electrode and close of the lower section. MnOOH thin-films deposited in this manner show flower-like structuring on the nanometer scale (figure 2.25). Coatings of manganese dioxide were grown to ~30nm thicknesses.

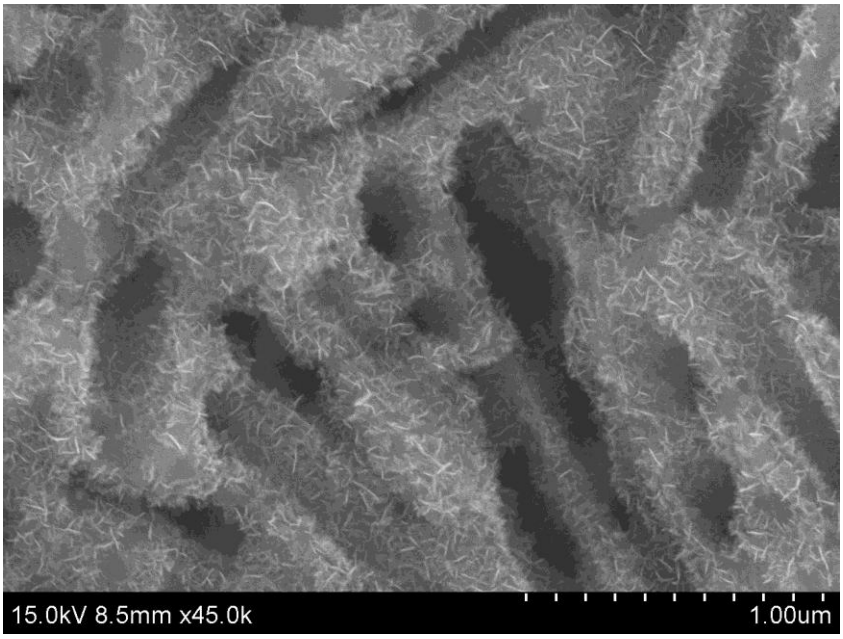

Figure 2.25. SEM image of MnOOH thin-film coating on nickel current collector.

The next step in fabricating the active material required lithiation of the MnOOH. A lithium salt bath was used to create the $LiMnO_2$ cathode. After, 1.7g of lithium hydroxide monohydrate (LiOH, Fisher Scientific, #L127) and 4.1g of lithium nitrate ($LiNO_3$, Sigma-Aldrich, #62575) were weighed and mixed in a ceramic crucible. After thorough grinding with a pestle for ~30 seconds, the lithium salt was poured into a beaker. The MnOOH/nickel composite samples were immersed in the lithium salt. The beaker of lithium salt was heated to ~300°C on a hot plate. During this process, the manganese dioxide dehydrates and lithium is inserted creating lithiated MnO_2. After ~30 minutes of immersion in the melted lithium salt, the sample was removed and salt residues were rinsed away with demonized water. The samples were thoroughly dried at ~70°C for ~8 hours. From this procedure, we have shown that we can fabricate thin films of active $LiMnO_2$ material coated on a nickel current collector with anisotropic architectures.

2.4.2 Electrochemical Analysis

After complete fabrication of the cathode, electrochemical analysis can assist in understanding the cathode's performance. An electrolyte solution composed of ~520mL dimethyl carbonate (DMC, Sigma-Aldrich, #517127, ≥99%), ~420mL ethylene carbonate (EC, Sigma-Aldrich, #676802, 99%), and lithium perchlorate ($LiClO_4$, Sigma-Aldrich, #62580, ≥98%) was made in an argon filled glove box. Electrochemical testing of lithium-ion cathode half cells were done in argon-based atmospheres to prevent lithium from violently reacting with moisture. A three electrode system was used to cycle the cathode. The counter electrode and reference electrode were each separate strips of lithium (Sigma-Aldrich, #265985, 99.9%). The cathodes underwent galvanostatic cycling (figure 2.26).

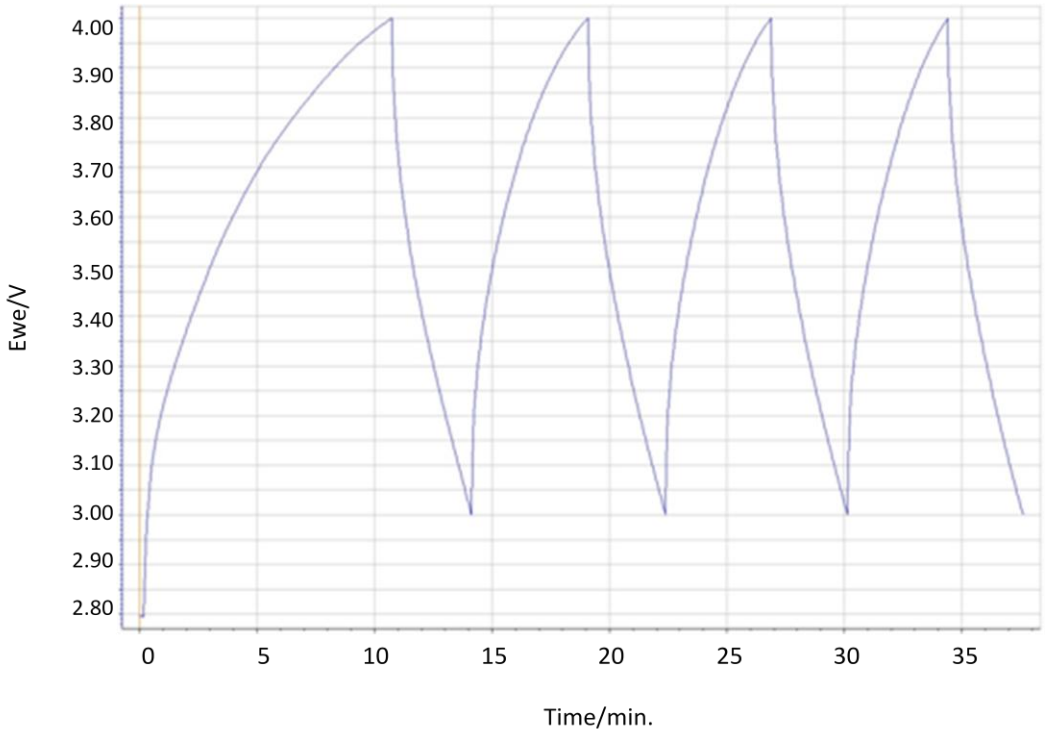

Figure 2.26. Galvanostatic cycling with potential limitation (GCPL) of $LiMnO_2$/nickel composite cycled against lithium. Four cycles of 0.01mA charge and discharges in a ~2.5-4.0V potential window.

The performance displayed in figure 2.26 shows an increase in potential during charging when the lithium is forced from the cathode to anode (lithium, in this half-cell configuration). During discharge, the lithium is chemically driven to shuttle back and intercalate into the active material of the cathode. The sample shown here does not demonstrate the high performance very well. This issue is most likely caused by a poor fabrication of the active material coating. Inadequate deposition of MnO_2 is most likely the culprit. Adjusting the cycling parameters of these MnO_2 electrodepositions to be more reproducible should be achievable. However, the electrochemical analysis does show that it works as a cathode. This demonstrates that bicontinuous $LiMnO_2$ cathodes with rod-shaped pores can be fabricated.

2.5 Future Directions

This research using anisotropic colloidal templates can be extended to a variety of future projects. The control of colloidal synthesis and template assembly allows one to manipulate the pore architectures. These pore architectures have an effect on the power density, energy density, and mechanical stability of the electrodes. With the large influences from the pore architectures, this research should inspire the use of anisotropic colloids in a variety of applications. The applications of these anisotropic colloidal templates may also be useful for other energy storage devices or even interesting photonic applications. Since the focus of this investigation is improving lithium-ion batteries, several related future directions will be suggested.

2.5.1 Further Analyses of Anisotropic Colloidal Templates

The pore architectures will affect the cathode performance. An interesting study would be a detailed investigation on the effect of tortuosity of the pore architectures. Colloidal crystals

(spherical particle templates) and vertically aligned anisotropic colloidal templates will produce cathodes with different pore architectures. Lithium ions traveling through the inverse opal structure will be more tortuous than direct pathways in the vertically aligned pores. However, the inverse opal maximizes its active material volume more than the rod-shaped pores, so there may be an interesting trade-off between the power and energy densities between these two scenarios. A couple other case studies might involve composites of spherical and rod particles of varying concentrations, and a study of the effect from pores' aspect ratios. These further analyses of anisotropic colloidal templates may be interesting scientific studies and open ideas to new applications.

2.5.2 Interdigitated Microbatteries

Interdigitated battery structures have anodes and cathodes that alternate between each other on a substrate. These systems may be more useful for microbattery applications since there is extended fabrication. There is current work on using anisotropic colloidal templates with horizontal alignment on the electrodes. By placing the SiO_2 colloid on the interdigitated fingers, an electric field can be applied to the electrodes (figure 2.27). With tuned electric field parameters particle alignment is perpendicular to the interdigitated fingers and parallel to the substrate surface. This alignment should produce pore architectures favorable to the direction of lithium transport. Another critical factor in this fabrication is the spacing and sizes between the gold electrode fingers. The particles will align best between the electrode fingers. By creating thin (~2μm) fingers with a taller heights, plating can mostly occur in the direction parallel to the surface of the electrodes. This can better utilize the particle templates that are more aligned between the fingers.

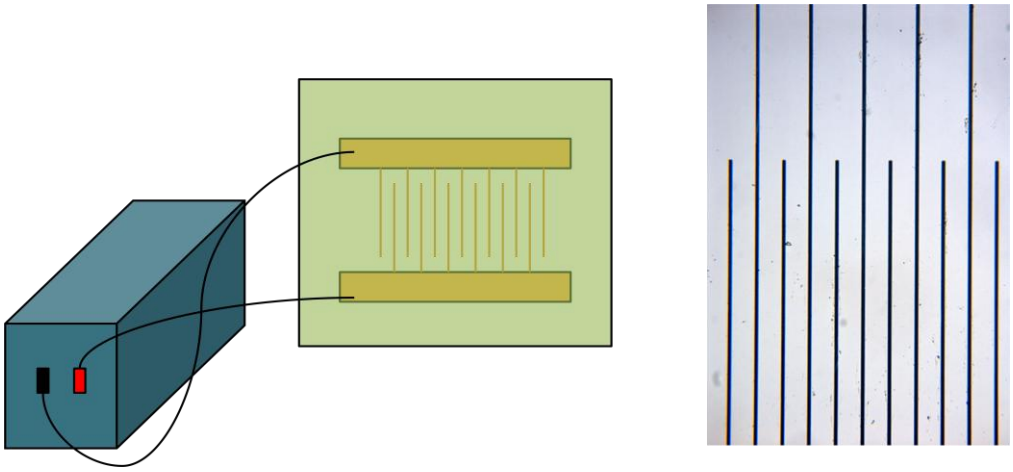

Figure 2.27. Left: schematic of function generator connected to the two electrodes of the interdigitated structure. Right: 10μm gold interdigitated fingers with 40μm spacing on glass substrate.

2.5.3 Silicon Anode Mechanical Stability

Although this thesis more specifically focuses on cathode designs for lithium-ion batteries, these anisotropic electrode structures may also provide usefulness for anode applications. Silicon is one of the more promising anode materials for lithium-ion batteries. About 1mol of silicon can react with about 4.4mol of lithium to form several intermediate Li-Si alloys. This ability corresponds to a super high capacity of 4000mAh/g. However during cycling, silicon shows volume expansions of nearly 400% [33, 34]. This expansion and contraction inherently leads to high stresses within the anode structure making it susceptible to mechanical failure. Previous work has been done creating honeycomb-structured silicon anodes using lithographic techniques [35]. These patterned structures are able to morphological change during lithiation (figure 2.28). It may be feasible to generate similar structures using aligned anisotropic colloidal templates that may show excellent cyclability.

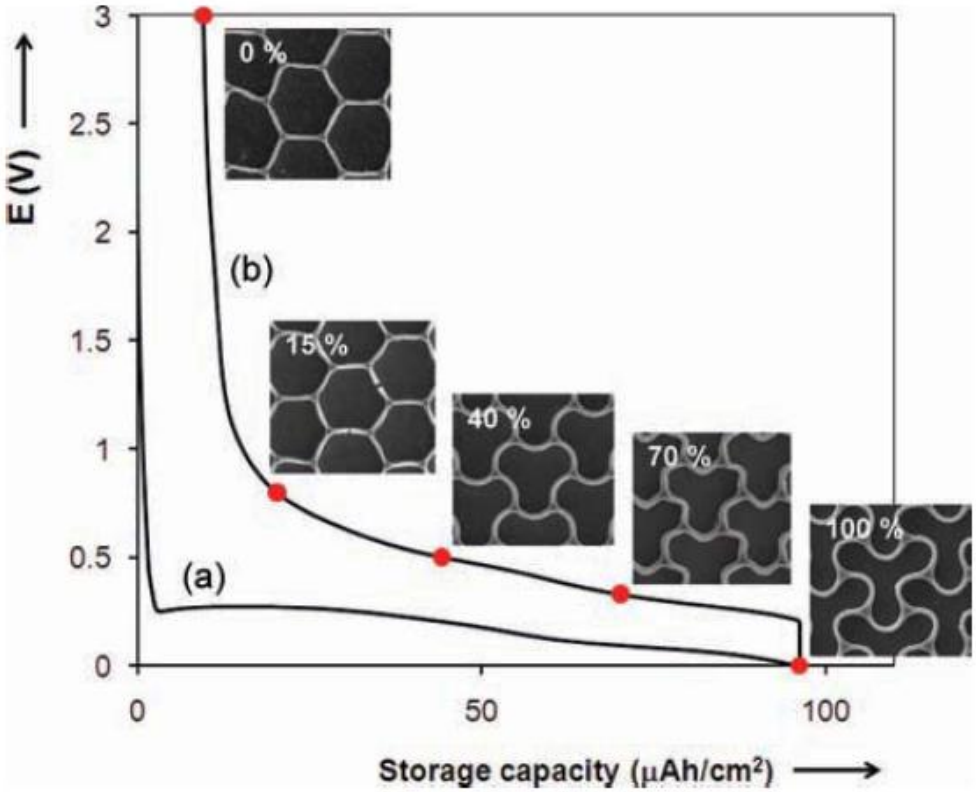

Figure 2.28. Morphological changes of silicon honeycomb structure as a function of lithium content. Figure adapted from “Honeycomb-Structured Silicon: Remarkable Morphological Changes Induced by Electrochemical De(Lithiation)” [35].

CHAPTER 3

THIN-FILM CATHODES OF ULTRA-HIGH ENERGY DENSITY MATERIALS

3.1 High Energy Capacity Materials for Lithium-ion Cathodes

In order to improve lithium-ion battery performance, cathodes must have an ideal structure (figure 1.3c). This structure requires thin films of active cathode material wrapped around a thin current collector with high porosity of interpenetrating networks. An ideal cathode structure has an active cathode material that has a small thickness, a high interfacial surface area with the electrolyte, and a high interfacial area with the current collector (figure 3.1). These characteristics increase in power densities. By wrapping these active material-current collector films into tight three-dimensional bicontinuous structures, the high power densities can still be achieved without sacrificing much energy density.

Figure 3.1. Schematic of an "ideal" cathode structure. Thin films of electrolytically active material (yellow/lighter) wrapped around a highly porous current collector (green/darker). Adapted from "Three-Dimensional Bicontinuous Ultrafast-Charge and –Discharge Bulk Battery Electrodes" [26].

This structural design seeks to improve cycling rate performance (~power density) while maintaining comparable energy densities. The lithium-ion battery cathodes fabricated by Zhang provide competitive power densities. The next step in improving these batteries is to address the

design with the goal of improving energy density. One might think that an easy way to do this is by increasing the thickness of the active material. However, doing this diminishes the cycling rate performance and does not offer fundamental, helpful design changes. The energy density of the lithium-ion cathode is dependent upon the type of active material and how much active material is there. Since it is desirable to keep similar active material thinness (to preserve low diffusion lengths), we limit ourselves to investigating new materials.

The active cathode material's energy density depends on the applied voltage and the capacitance of the material (the amount of charge able to be extracted). If the applied voltage is too high, new design challenges may ensue. These may include electrolyte and separator voltage breakdowns and uncontrollable oxidation reactions within other battery components. So the best way to improve energy densities is by using new materials with high specific capacitances (figure 3.2).

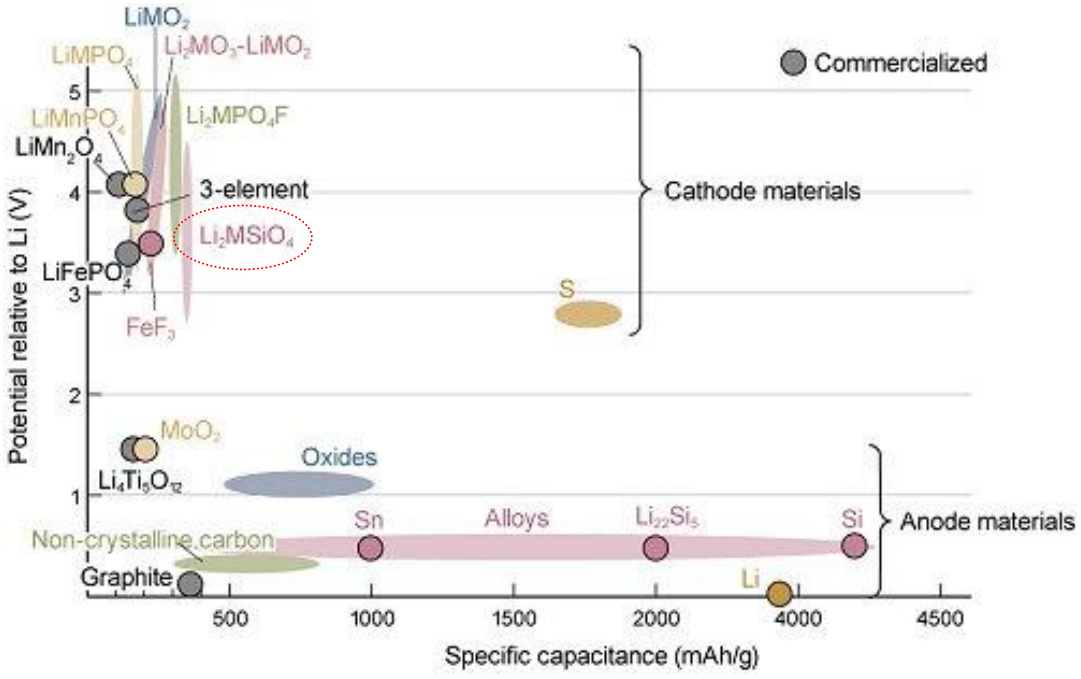

Figure 3.2. Plot cathode and anode materials based upon gravimetric specific capacitance versus potential relative energy capacities. Adapted from "The First Step is New Materials to Boost Capacity" [36].

3.2 Li_2MSiO_4 Materials

A new class of polyoxyanion cathodes based on the orthosilicates, Li_2MSiO_4 (where M = Mn^{2+}, Fe^{2+}, and Co^{2+}), have been attracting significant attention. These materials are based upon silicon, and some iron, which are some of the most abundant and low costing elements. The structure is based upon very strong and stable Si-O bonds that promote similar lattice stabilization effects to the phosphate bonds found in $LiFePO_4$. These materials provide cheap, safe, and sustainable active cathode materials, some of the prime targets in large scale lithium batteries. However, the most attractive feature of this material is its ultra-high specific capacity [37-44]. These polyoxyanion orthosilicate systems work on a two-electron system. The first electron extracted from Li_2MSiO_4 works on the M^{2+}/M^{3+} redox couple such that:

$$Li_2M^{(2+)}SiO_4 \leftrightarrow LiM^{(3+)}SiO_4 + 1Li^+ + 1e^-$$

Most lithium intercalation cathodes extract only one lithium ion per molecule, which means only one corresponding electron is extracted. However in the Li_2MSiO_4 systems, a second electron may be extracted utilizing the M^{3+}/M^{4+} redox couple:

$$Li_2M^{(3+)}SiO_4 \leftrightarrow M^{(4+)}SiO_4 + 2Li^+ + 2e^-$$

Since this second electron can be extracted from the molecule, more electric charge can be stored in the battery. This two-electron system provides the Li_2MSiO_4 theoretical specific capacities of around ~333mAh/g. Since most of these systems apply potentials of up to ~4.5V (against lithium), these materials may provide ultra-high energy density required for lithium-ion battery performance. To utilize this high energy density material, and preserve a high power density, methods to create thin films of Li_2MSiO_4 on bicontinuous current collectors will be investigated. First, it is important to thoroughly understand Li_2MSiO_4 materials in order to design an advanced battery cathode system.

3.2.1 Structure and Properties

The structure of Li_2MSiO_4 materials can be associated with lithiophosphate-type (Li_3PO_4) structures (figure 3.3) [38]. The structure is first composed of silicon dioxide tetrahedra, SiO_4. The Si-O has exceptionally strong bonding which provides the Li_2MSiO_4 with lattice stability [40]. This lattice stability is critical since lithium ions move in and out of the active material, inducing lattice strains. Metal (Mn, Fe, or Co) oxide tetrahedra alternate with the silica tetrahedra. The transitional metals (Mn, Fe, or Co) within these tetrahedra form ionic bonds with the lithium. As lithium is extracted from the material, the transitional metal can change its valence and produce an electron for every lithium ion extracted [41].

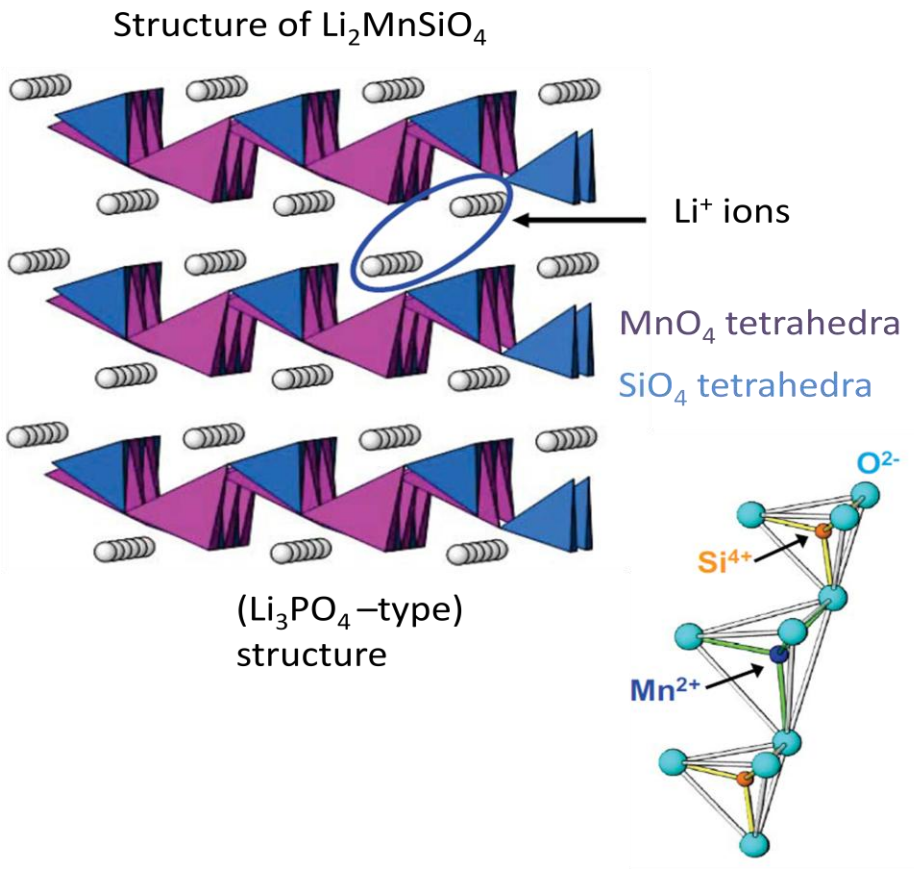

Figure 3.3. Schematic of Li_2MnSiO_4 structure, Li_3PO_4 – type structure. $[Mn^{(x+)}O_4]$ and $[SiO_4]$ alternating tetrahedra provide the physical structure of the material system. Manganese shares bonding with lithium ions and can change its valence as lithium extracts/inserts. Figure adapted from "Evaluation of Li_2MnSiO_4 Cathode" [39].

Due to the theoretical >1 electron extraction, Li_2MSiO_4 materials have theoretically ultra-high energy capacities of greater than ~300mAh/g. Applied potentials of around ~3.6V is enough to pull out the first lithium ions. The second electron will not be witnessed until the Li_2MSiO_4 applied voltages are at least ~4.5V. Capacitances above ~190mAh/g will prove that second electron extraction is occurring. However, only some have found this phenomenon to occur [42], and have only seen up to ~1.2 electrons extracted. These materials are also infamously known for their low electronic conductivities. These basic properties are critical to understand to have a sense about the results of any experimentation.

3.2.2 Conventional Fabrication Techniques

It may be desirable to adapt a well-established synthesis route and apply it to the advanced cathode structures. Most (~96%) of the published synthesis procedures involve a wet-state sol-gel synthesis [37-39, 42-45]. The sol-gel process is a wet chemical technique used for fabrication of ceramic materials, often active battery materials [46, 47]. In these processes, wet-state chemical precursors of metal alkoxides or metal chlorides are first prepared. These precursors are mixed and chelated, and further undergo polycondensation and hydrolysis to form a colloid. These Li_2MSiO_4 colloids form chain like polymer networks. After thorough gelation, the Li_2MSiO_4 gels are dried completely and calcinated at high temperatures which remove organic ligands and form the Li_2MSiO_4 materials into proper crystal structures. The basic outline of these fabrication techniques is wet-chemical preparation, sol-gel transformation, and subsequent calcination. It is desirable to utilize this fabrication and adapt it to form thin films of Li_2MSiO_4 on bicontinuous current collector structures.

3.3 Li_2MnSiO_4 Sol-Gel Dip-Coating Method

Sol-gel dip-coating is a common method to make thin-film glass and ceramic material coatings [48, 49]. The current collectors of the high-performance cathodes are nickel structures high porosity and interpenetrating networks. To improve the design of lithium-ion cathodes, thin films of high energy density active material should be deposited on the advanced current collector structures. In this section, sol-gel dip-coating techniques are explored for creating thin films of Li_2MnSiO_4 on the nickel current collectors. Of the Li_2MSiO_4 family, lithium manganese orthosilicate (Li_2MnSiO_4) was the only material experimented with. Although, the iron-based silicates and cobalt-based silicates have their own advantages, manganese-based silicates have had the best results in high capacity [38-41, 43] in previous reports.

3.3.1 Synthesis of Li_2MnSiO_4

The synthesis of the Li_2MnSiO_4 solution was based on procedures adapted from Dominko [41]. However, several steps were modified. Successful synthesis of the material first required properly cleaned glassware. All glassware, including flasks, glass vials, and funnels were initially cleaned with detergents, water, and organic solvents. Next, the glassware was left in base bath for at least seven hours. Once removed from the base bath, the glassware was rinsed with copious amounts of Millipore water (resistivity at 18.2MΩ). The rinsed glassware was kept in a clean oven at 120-140°C until used.

The most important step of this synthesis is creating the proper cationic molar ratio of 2:1:1 for Li:Mn:Si. The first step in the synthesis is to prepare three separate solutions that will each provide the lithium, manganese, and silicon cations to the final ceramic. In a 130mL beaker, 7.652g of lithium acetate dihydrate (LiAc, Sigma-Aldrich, #L4158) and 100mL of Millipore

water were mixed with a magnetic stir bar for ~30 minutes until completely dissolved. In a separate 130mL beaker, 9.191g of manganese (II) acetate tetrahydrate ($MnAc_2$, Sigma-Aldrich, #63537, ≥99.0%) was mixed with 100mL of Millipore, and stirred until completely dissolved. The beaker is where the silica is prepared. Similar syntheses use silica particles of sizes ~100-300nm in diameter. However, here commercial silica dispersion with silica particles of 7nm in size is used. In the third mixture, 7.51g of silica dispersion (LUDOX® SM-30 colloidal silica, 30wt% suspension in H_2O, Sigma-Aldrich, #420794) and 367.5mL of Millipore were mixed and sonicated for ~1hr in a sonication bath. After sonication, 2.402g of citric acid (CA, Acros Organics, #42356, 99.5%) and 2.328g of ethylene glycol (EG, Sigma-Aldrich, #324558, 99.8%) are added to the silica colloid. After another hour of sonication, the silica mixture, dissolved LiAc, and dissolved $MnAc_2$, were all mixed into a 1000mL flask. The flask was covered and stirred with a magnetic stirrer for ~3 hours under ambient conditions.

At this point, the solution is ready to be applied for a sol-gel dip-coating process (next section). The rest of this section will describe the gelation process and other related experiments/results. To gelate the Li_2MnSiO_4 solution, the 1000mL flask was heated to 60°C. After approximately half of the solution was evaporated, the solution was transferred a crystallizing dish and kept at 60°C on a hot plate. After a total of ~12-18hours, the solution turned into a hardened gel. The hardened gel was transferred to a mortar and pestle and thoroughly ground to a fine powder. The powder was place into an alumina boat and calcinated at 700°C in forming gas for 6 hours. The calcination, and organic burnout, was done in a horizontal convection furnace. After, the particles sizes were analyzed using a scanning electron microscope (figure 3.4). The particles, without post-calcination grinding, were ~50-100nm diameter.

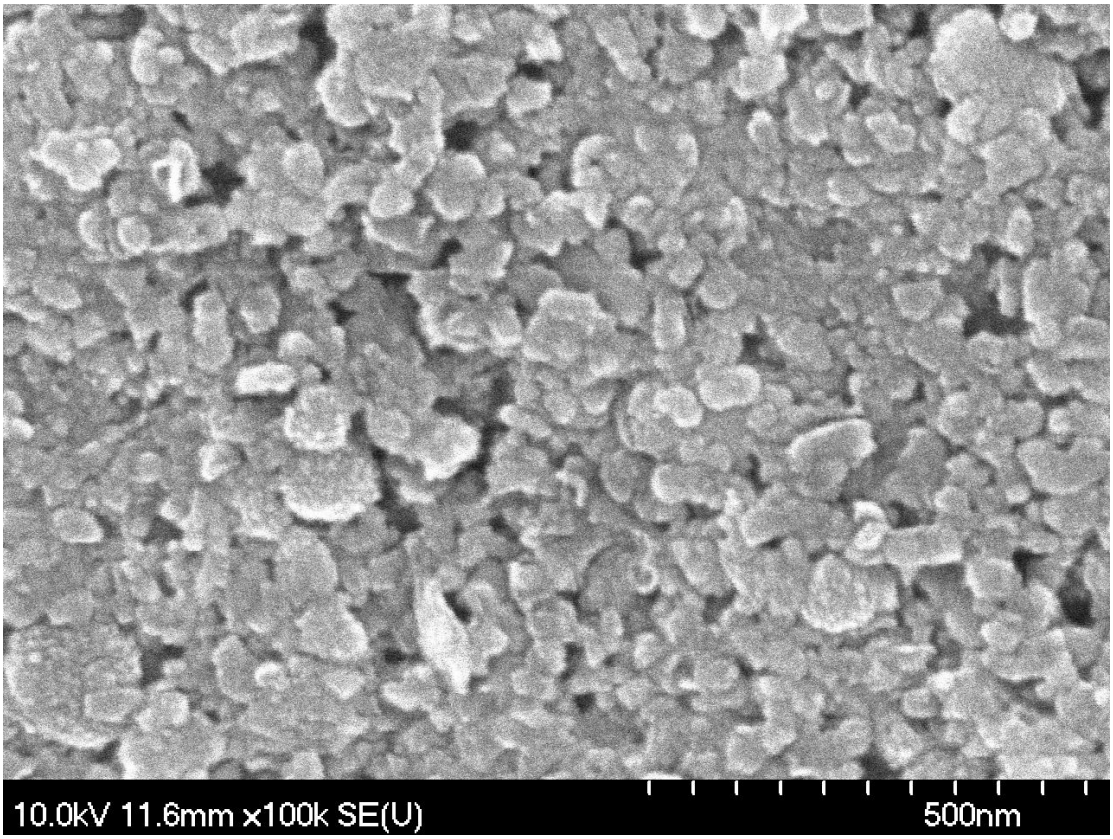

Figure 3.4. SEM image of Li_2MnSiO_4 nanoparticles (~50-100nm diameter) synthesized via modified sol-gel route.

The goal is to use this synthesis method for a sol-gel dip-coating technique. Since the nickel current collector structures will begin to fail at a certain temperature, it is critical to know the temperature required for calcination. Several samples were calcinated in forming gas (95%Ar, 5%H_2) for 6 hours. Three samples, 500°C, 600°C, and 700°C calcinations, were separately prepared. The samples were then prepared for powder x-ray diffraction (XRD, Siemens-Bruker D5000 XRD). Compared to simulated XRD information, calcinations of 600°C and up show similar crystal structure with the simulated information (figure 3.5). Lower calcination temperatures may provide easier fabrication routes of the active material on the current collector. However, the trade-off shows higher percentages of impurities at lower

calcinations. From Jade X-ray Analysis, 700°C, 600°C, and 500°C showed impurity levels of ~3%, ~5%, and ~12%, respectively. Depending on the amount of required purity, different calcinations may be used for the Li_2MnSiO_4.

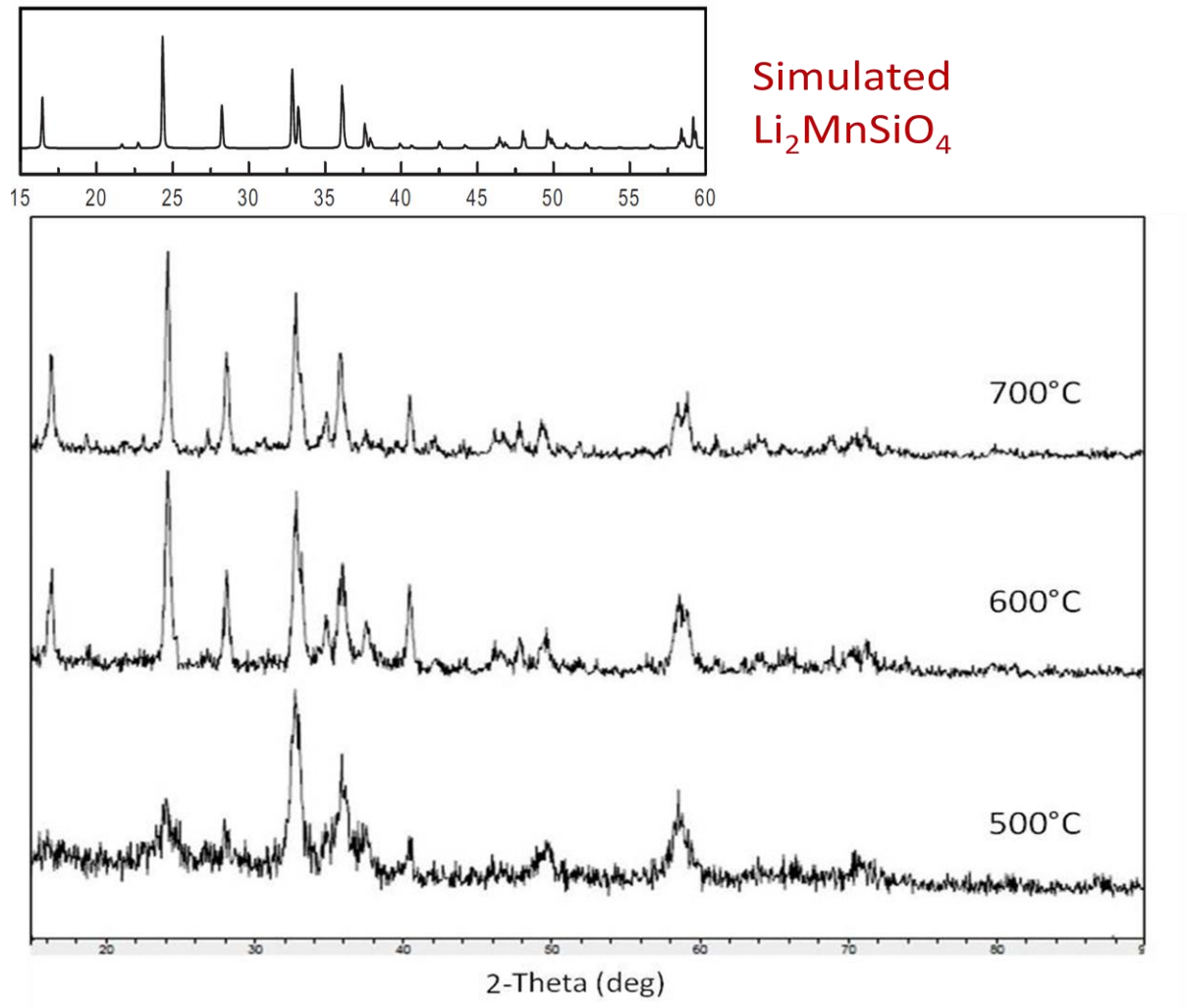

Figure 3.5. X-ray diffraction patterns of Li_2MnSiO_4 after calcination in forming gas of three different temperatures: 500°C, 600°C, and 700°C. 500°C sample shows relatively high amount of impurities of MnO, Mn_2SiO_4, and Li_2SiO_3. 2-Theta scans from 15 to 90 degrees. Simulated XRD pattern of Li_2MnSiO_4; 2-Θ scans from 15 to 60 degrees. Simulated data adapted from "Evaluation of Li_2MnSiO_4 Cathode" [39].

3.3.2 Dip-Coated Bicontinuous Cathode

A Li_2MnSiO_4 bicontinuous cathode can be fabricated using a sol-gel dip-coating process. During a dip-coating process, the current collector is immersed in the sol-gel solution. As the sample is removed, Li_2MnSiO_4 colloidal particles (with their polymer ligands) should adhere to the surface of the substrate. During gelation, the Li_2MnSiO_4 solution changes in viscosity during the gelation-evaporation process. This viscosity change can be utilized to adjust film thicknesses created during dip-coating. Microporous nickel foam (pore sizes ~200-500μm) was cut into ~0.5in by ~1in pieces. The foam was immersed into the solution (after ~2 hours of evaporation at 60°C) for ~1s, and slowly removed afterwards. After drying the sample in ambient conditions for ~1hr, the sample was calcinated at 500°C in forming gas for 6 hours. This produced a thin film (~80nm thick) of Li_2MnSiO_4 onto the nickel foam current collector (figures 3.6, 3.7, and 3.8).

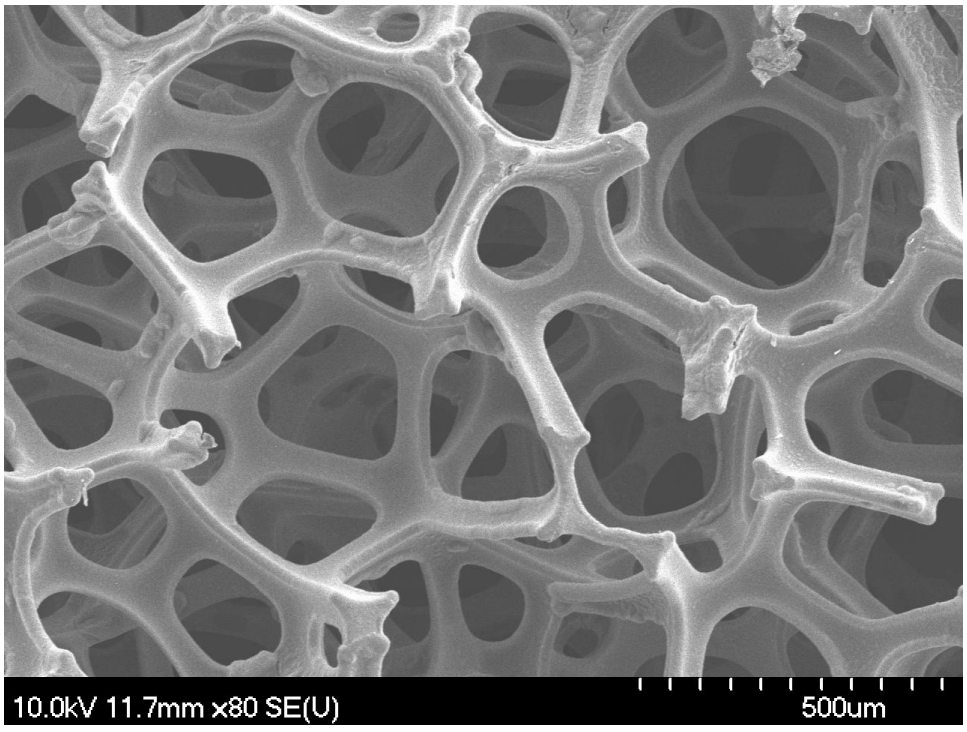

Figure 3.6. SEM image of Li_2MnSiO_4 nanoparticles coated on nickel foam. This is the 2hr-evaporated solution. Samples were calcinated at 500°C for 6hr in forming gas.

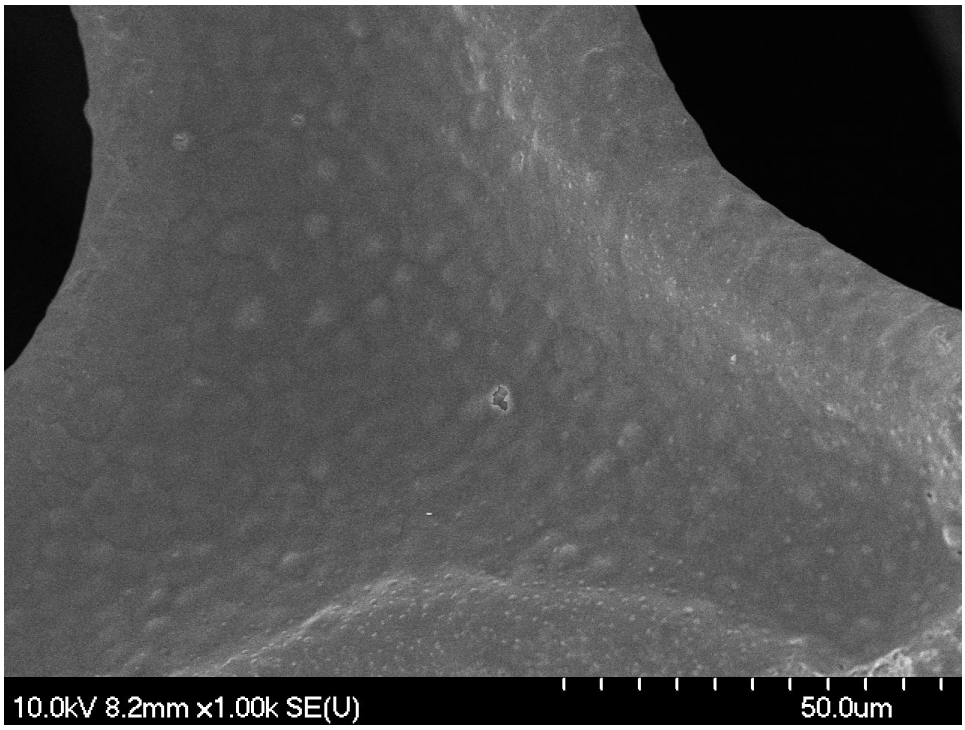

Figure 3.7. SEM image of Li_2MnSiO_4 nanoparticles coated on nickel foam. This is the 2hr-evaporated solution. Samples were calcinated at 500°C for 6hr in forming gas.

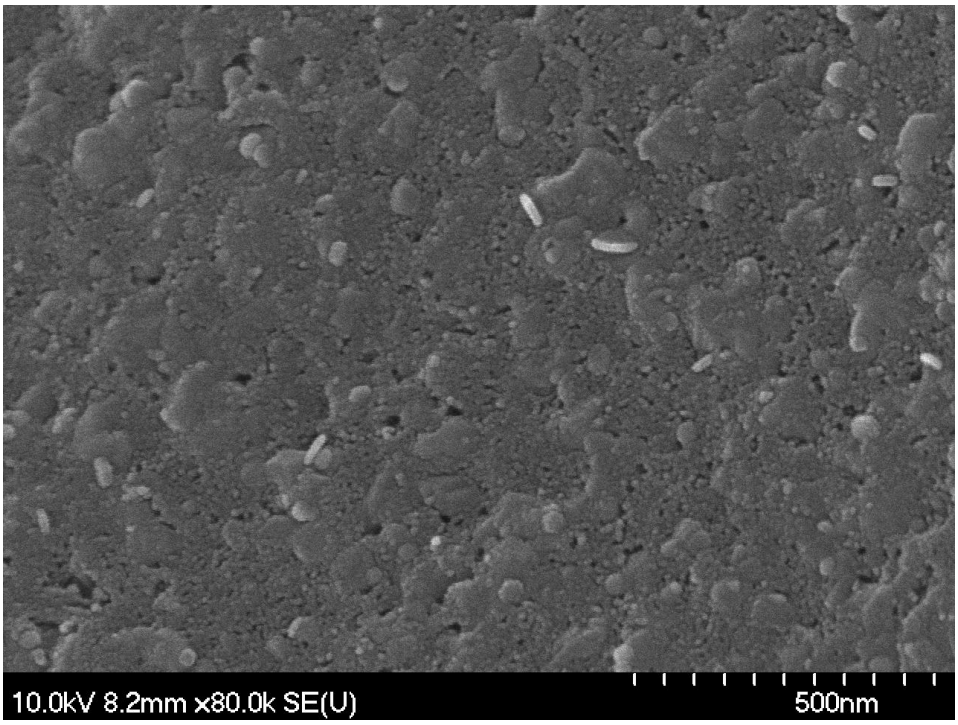

Figure 3.8. SEM image of Li_2MnSiO_4 nanoparticles coated on nickel foam. This is the 2hr-evaporated solution. Samples were calcinated at 500°C for 6hr in forming gas.

After preparing the cathodes, they were electrochemically tested to analyze their performance. Electrolyte solution, based upon DMC, EC, and $LiClO_4$ (preparation described in section 2.4.2) was used. Several samples were dip-coated at varying viscosities of the sol-gel. These samples included 0hr, 4hr, and 21hr sol-gel evaporation times. These will each correspond to a viscosity, increasing in increased evaporation times. However, electrochemical GCPL showed no trends/differences. Each solution samples were tested at 1mA, 0.5mA, and 0.25mA rates. Higher current rates yielded lower capacities, as expected. However, all of the samples showed low capacities (figure 3.9).

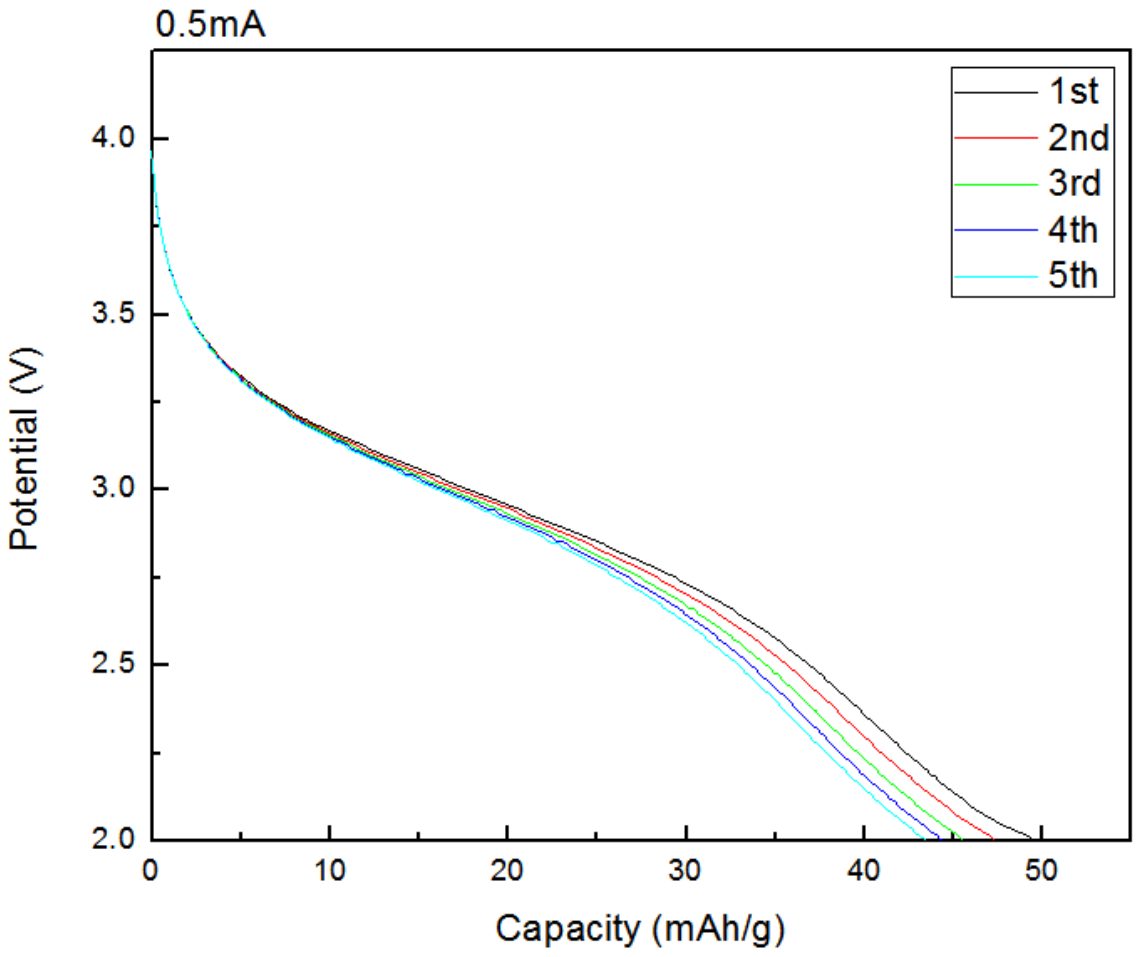

Figure 3.9. Discharge profile of Li_2MnSiO_4/nickel foam cathode for five cycles. 0.5mA charge and discharge rates show capacities around ~47mAh/g.

The performances showed capacities from ~40-70mAh/g. Although only few previous reports have witnessed capacities that show >1 electron extraction [45], most other investigations show at least ~160mAh/g capacities. Some speculations can be made regarding the low performance. Samples calcinated at 500°C in forming gas produced impurities of up to ~12%. However, these samples were calcinated onto nickel current collectors. The nickel/Li_2MnSiO_4 interface may produce more impurities. For instance, if nickel has a higher affinity to oxygen at these temperatures, the active material may be made with manganese not in its +2 valence. Even without additional impurities from the nickel, these impurities may exponentially reduce the electron and ionic conductivities required for high-performance. Although performance was low here, a sol-gel dip-coating technique was demonstrated to produce thin films of (theoretically) ultrahigh energy density active cathode materials.

3.4 Future Directions

This project investing thin-film coatings of Li_2MnSiO_4 on bicontinuous current collectors can be extended into a variety of future directions. The low capacity of this material seen here can be further investigated in the hope of improving it. These materials may be better understood by some control experiments on Li_2MnSiO_4 electrical conductivity. The materials might also be improved by modifying the sol-gel synthesis described earlier. However, improving the material properties is not the only goal of these investigations. The other main goal of these investigations is to fabricate the active materials into thin films on bicontinuous structures. Modifying the sol-gel dip-coating technique or other chemical vapor deposition processes may provide a route for depositing Li_2MnSiO_4 active materials onto bicontinuous current collectors.

3.4.1 Control Experiments on Li_2MnSiO_4 Electronic Conductivity

The biggest issue with Li_2MnSiO_4 is its low electrical conductivity [37-39, 44]. There have not been any control experiments on the material's electrical conductivity. Poor electrical conductivity implies that the electrons travelling through the material need relatively high potentials. However, if the material is thin enough, the effects from poor electrical conductivity may be diminished. A control experiment on film thickness/electrical conductivity may provide insight to developing Li_2MnSiO_4 cathodes.

The Li_2MnSiO_4 should first be prepared using the sol-gel process described above. After calcination, the powder should be thoroughly ground into a finer powder. Ball-mill grinding may help produce small nanoparticles of the Li_2MnSiO_4 material. Once the Li_2MnSiO_4 is prepared into a nanoparticle powder, it should be filtered to improve its monodispersity. Carbon black particles should also be prepared into nanoparticle powders. The carbon black powder has extremely high electronic conductivity. Many cathodes made via conventional casting of films of active material mix 5-10% carbon powder to improve the electrical conductivity.

The Li_2MnSiO_4 and carbon nanoparticle powders should be mixed in various concentrations. The samples of varying concentrations should be prepared and casted into conventional cathodes. Increasing the concentration of carbon effectively produces smaller thickness of Li_2MnSiO_4. If the nanoparticles are prepared small enough in size, the compositions with high carbon concentration will effectively behave as a ~20nm (dependent on particle size and concentration) thick film. Electrochemical analysis and normalization to the concentration of Li_2MnSiO_4 can provide some insight to the capacity. If the electrical conductivity is high enough, the specific capacity may be closer to its theoretical predictions.

3.4.2 Multi-Layer Syntheses

As noted before, most publications have only explored sol-gel – type fabrications of Li_2MnSiO_4 active materials. Sol-gel dip-coating worked well to create Li_2MnSiO_4 bicontinuous cathode materials on nickel foam current collectors. To improve the energy density (normalized to the volume of the entire cathode), this process was tested on nickel inverse opal structures of ~1.8μm pore sizes. The dip-coating process did not produce conformal coatings of the active material. Instead of sol-gel dip coating another process to create thin-films of Li_2MnSiO_4 could be investigated.

Figure 3.10 shows a ternary phase diagram of silica, manganese oxide, and lithium oxide. This ternary phase diagram illustrates the difficulty in synthesis a four-element ceramic compound with correct stoichiometry. A number of impurities can, and are often produced during Li_2MnSiO_4 synthesis. However, these types of phase diagrams might also give some insight into new syntheses. Chemical vapor deposition of manganese and silica has been previously demonstrated [50-54]. Multi-layer chemical vapor depositions of these two with a subsequent lithiation process may be one way to coat Li_2MnSiO_4 active materials onto inverse opal structures.

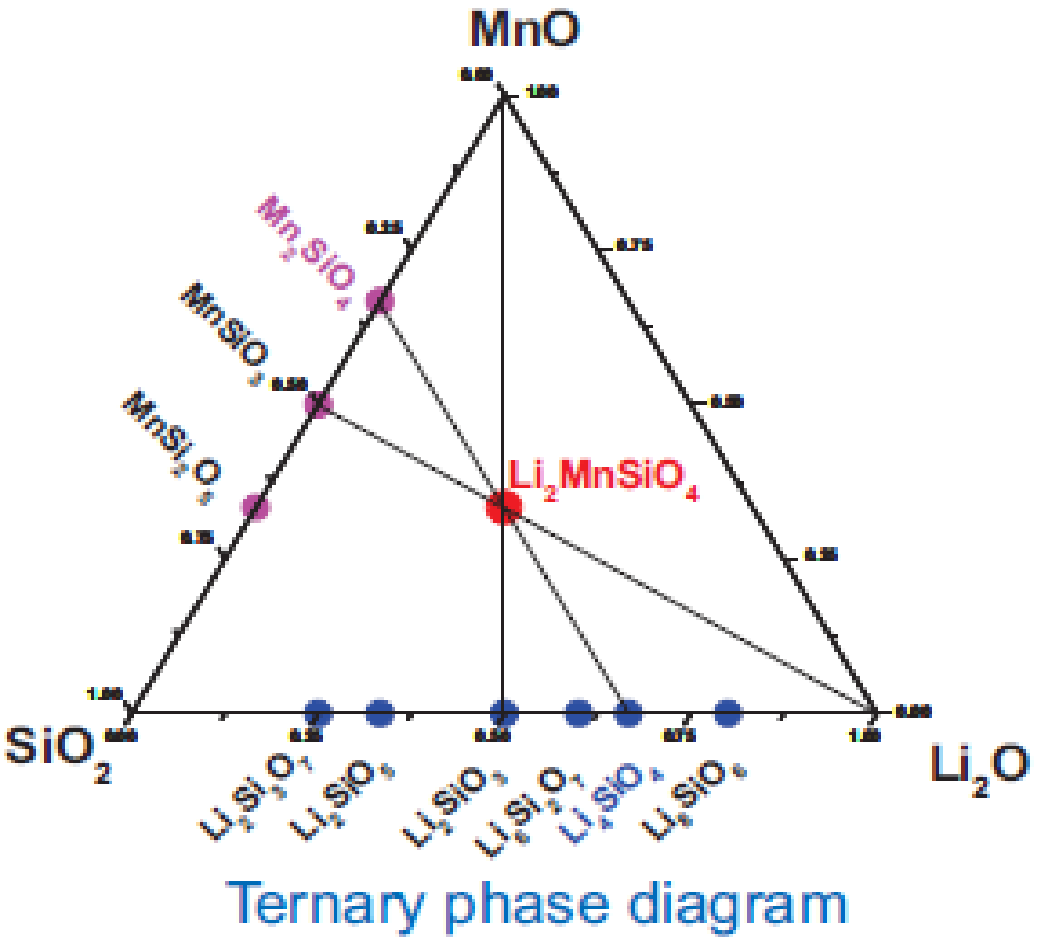

Figure 3.10. Ternary phase diagram of silica (SiO_2), manganese oxide (MnO), and lithium oxide (Li_2O). Diagram shows a variety of phases possible and Li_2MnSiO_4 as the phase equally composed of the three intial molecular phases. Adapted from "Evaluation of Li_2MnSiO_4" [39].

CHAPTER 4

CONCLUSIONS

Advanced lithium-ion battery cathodes require three-dimensional bicontinuous structures to improve the cycling rate performances while maintaining a considerable energy density. The pore architectures of the bicontinuous design should affect the charging and discharging rates. This investigation demonstrates the ability to control the pore architectures of advanced cathode structures. Silicon dioxide rod-shaped particle colloids are synthesized. This synthesis provides dimensional control over the particle sizes, and reproducible monodispersity. Using the silica colloids, alternating-current electric fields and casting techniques are used to create anisotropic colloidal templates for electrode current collector fabrication. These assembly techniques create templates with perpendicular, parallel, and purely random orientations. Nickel was electrodeposited through the templates and the silica particles were etched afterwards. This work lays out a pathway for fabricating electrodes with controllable pore architectures. Lithiated manganese dioxide thin films were deposited onto the nickel current collectors. Electrochemical analysis does not yet confirm structural influences on power density. This process of creating anisotropic colloidal templates for directional current collector novel architectures may be applicable to a variety of energy storage systems.

Three-dimensional bicontinuous structures provide cathodes with high power density and maintain the energy density. To increase the energy densities of these cathode systems, structural refinements may only offer small improvements. Novel Li_2MnSiO_4 active cathode materials theoretically provide ultrahigh specific capacitances that may help improve energy densities. The Li_2MnSiO_4 materials were synthesized and further fabricated into advanced structures. Sol-gel dip-coating methods were investigated for depositing the active materials onto porous nickel

foams. Conformal coating of the materials on the foam was achieved using the dip-coating method. Conformal coatings of Li_2MnSiO_4 onto nickel inverse opals were not reproducible. Li_2MnSiO_4 dip-coating may not be feasible at these structural dimensions. This research lays out the groundwork for further inquiry into designing advanced lithium-ion cathodes. These cathode architectures and materials provide novel designs to improve lithium-ion battery power and energy densities.

REFERENCES

[1] Horiba, T.; Maeshima, T.; Matsumura, Koseki, M.; Arai, J.; Murananka, Y., Applications of High Power Density Lithium Ion Batteries. *Journal of Power Sources* **2005**, *146*, 107-110.

[2] Johnson, B. A.; White, R. E., Characterization of Commercially Available Lithium-ion Batteries. *Journal of Power Sources* **1998**, *70*, 48-54.

[3] Huggins, R. A., *Advanced Batteries: Materials Science Aspects* 1ed.; Springer, LLC: New York, NY, 2009.

[4] Christen, T.; Carlen, M. W., Theory of Ragone Plots. *Journal of Power Sources* **2000**, *91*, 210-216.

[5] Flynn, P. and et al., *Meeting the Energy Needs of Future Warriors*, Committee on Soldier Power/Energy Systems, Board on Army Science and Technology, National Research Council of the Nation Academies, Ed. The National Academies Press, 2004.

[6] Bruce, P. G.; Scrosati, B.; Tarascon, J.-M., Nanomaterials for Rechargeable Lithium Batteries. *Angewandte Chemie International Edition* **2008**, *47*, 2930-2946.

[7] Scriven, L.E., Equilibrium Bicontinuous Structure. *Nature* **1976**, *263*, 123-125.

[8] Cui, L.-F.; Yang, Y.; Hsu, C.-M.; Cui, Y., Carbon-Silicon Core-Shell Nanowires as High Capacity Electrode for Lithium Ion Batteries. *Nano Letters* **2009**, *9 (9)*, 3370-3374.

[9] Doherty, C. M.; Caruso, R. A.; Smarsly, B. M.; Adelhelm, P.; Drummond, C. J., Hierarchically Porous Monolithic $LiFePO_4$/Carbon Composite Electrode Materials for High Power Lithium Ion Batteries. *Chemistry of Materials* **2009**, *21 (9)*, 5300-5306.

[10] Herzig, E. M.; White, K. A.; Schofield, A.B.; Poon, W. C. K.; Clegg, P.S., Bicontinuous Emulsions Stabilized Solely by Colloidal Particles. *Nature Materials* **2007**, *7*, 966-971.

[11] Stratford, K.; Adhikari, R.; Pagonabarraga, I.; Desplat, J.-C.; Cates, M. E., Colloidal Jamming at Interfaces: A Route to Fluid-Bicontinuous Gels. *Science* **2005**, *309*, 2198-2201.

[12] Yabu, H.; Hirai, Y.; Shimomura, M., Electroless Plating of Honeycomb and Pincushion Polymer Films Prepared by Self-Organization. *Langmuir* **2006**, *22 (23)*, 9760-9764.

[13] Schaedler, T. A.; Jacobsen, A. J.; Torrents, A.; Lian, J.; Greer, J. R.; Valdevit, L.; Carter, W. B., Ultralight Metallic Microlattices. *Science* **2011**, *334*, 962-965.

[14] Lee, M. N.; Mohraz, A., Bicontinuous Macroporous Materials from Bijel Templates. *Advanced Materials* **2010**, *22*, 4826-4841.

[15] Pugh, D. V.; Dursun, A.; Corcoran, S. G., Formation of Nanoporous Platinum by Selective Dissolution of Cu from $Cu_{0.75}Pt_{0.25}$. *Journal of Materials Research* **2002**, *18 (1)*, 216-221.

[16] Fritz, J. D.; Pickering, H. W., Selective Anodic Dissolution of Cu-Au Alloys: TEM and Current Transient Study. *Journal of The Electrochemical Society* **1991**, *138 (11)*, 3209-3218.

[17] Pryor, M. J.; Fister, J. C., The Mechanism of Dealloying of Copper Solid Solutions and Intermetallic Phases. *Journal of The Electrochemical Society* **1984**, *131 (6)*, 1230-1235.

[18] Gardiazabal, J. I.; Galvele, J. R., Selective Dissolution of Cd-Mg Alloys. *Journal of The Electrochemical Society* **1980**, *127 (2)*, 259-265.

[19] Li, R.; Sieradzki, K., Ductile-Brittle Transition in Random Porous Au. *Physical Review Letters* **1992**, *68 (8)*, 1168-1171.

[20] Ding, Y.; Kim, Y. J.; Erlebacher, J., Nanoporous Gold Leaf: "Ancient Technology"/Advanced Material. *Advanced Materials* **2004**, *16 (21)*, 1897-1900.

[21] Shir, D. J.; Nelson, E. C.; Chanda, D.; Brzezinski, A.; Braun, P. V.; Rogers, J. A., Dual Exposure, Two-Photon, Conformal Phase Mask Lithography for Three Dimensional Silicon Inverse Woodpile Photonic Crystals. *Journal of Vacuum Science and Technology B: Microelectronics and Nanometer Structures* **2010**, *28*, 783-788.

[22] Miyake, M.; Chen, Y.-C.; Braun, P. V.; Wiltzius, P., Fabrication of Three-Dimensional Photonic Crystals Using Multibeam Interference Lithography and Electrodeposition. *Advanced Materials* **2009**, *21*, 3012-3015.

[23] Lewis, J. A.; Direct Writing of 3D Functional Materials. *Advanced Functional Materials* **2006**, *16*, 2193-2204.

[24] Direct-Write Assembly of Three-Dimensional Photonic Crystals: Conversion of Polymer Scaffolds to Silicon Hollow-Woodpile Structures. *Advanced Materials* **2006**, *18*, 461-465.

[25] Yu, X.; Lee, Y. J.; Furstenberg, R.; White, J. O.; Braun, P. V., Filling Fraction Dependent Properties of Inverse Opal Metallic Photonic Crystals. *Advanced Materials* **2007**, *19*, 1689-1692.

[26] Zhang, H.; Yu, X.; Braun, P. V., Three-Dimensional Bicontinuous Ultrafast-Charge and -Discharge Bulk Battery Electrodes. *Nature Nanotechnology* **2011**, *6*, 277-281.

[27] Jiang, P.; Bertone, J. F.; Hwang, K. S.; Colvin, V. L., Single-Crystal Colloidal Multilayers of Controlled Thickness. *Chemistry of Materials* **1999**, *11 (8)*, 2132-2140.

[28] Kuijk, A.; van Blaaderen, A.; Imhof, A., Synthesis of Monodisperse, Rodlike Silica Colloids with tunable Aspect Ratio. *Journal of American Chemical Society* **2011**, *133*, 2346-2349.

[29] Zhang, J.; Liu, H.; Wang, Z.; Ming, N., Au-Induced Polyvinylpyrrolidone Aggregates with Bound Water for the Highly Shape-Selective Synthesis of Silica Nanostructures. *European Journal of Chemistry* **2008**, *14*, 4374-4380.

[30] Trau, M.; Saville, D. A.; Aksay, I. A., Field-Induced Layering of Colloidal Crystals. *Science* **1996**, *272*, 706-709.

[31] Mantegazza, F.; Caggioni, M.; Jiménez, M. L.; Bellini, T., Anomalous Field-Induced Particle Orientation in Dilute Mixtures of Charged Rod-Like and Spherical Colloids. *Nature Physics* **2005**, *1*, 103-106.

[32] O'Konski, C. T., Molecular Electro-Optics, Part 1-Theory and Methods. *Journal of Polymer Science: Polymer Letters Edition* **1978**, *16 (11)*, 615-616.

[33] Obrovac, M. N.; Christensen, L., Structural Changes in Silicon Anodes during Lithium Insertion/Extraction. *Electrochemical and Solid-State Letters* **2004**, *7*, A93-A96.

[34] Lee, S. J.; Lee, J. K.; Chung, S. H.; Lee, H. Y.; Lee, S. M.; Baik, H. K., Stress Effect on Cycle Properties of the Silicon Thin-Film Anode. *Journal of Power Sources* **2001**, *97-98*, 191-193.

[35] Baggetto, L.; Danilov, D.; Notten, P. H. L., Honeycomb-Structured Silicon: Remarkable Morphological Changes Induced by Electrochemical (De)Lithiation. *Advanced Materials* **2011**, *23*, 1563-1566.

[36] Kariatsumari, K.; Kume, H.; Yomogita, H.; Keys, P., "The Step is New Materials to Boost Capacity". *Nikki Electronics Asia*, February 2010.

[37] Islam, M. S.; Dominko, R.; Masquelier, C.; Sirisopanaporn, C.; Armstrong, A. R.; Bruce, P. G., Silicate Cathodes for Lithium Batteries: Alternatives to Phosphates?. *Journal of Materials Chemistry* **2011**, *21*, 9811-9818.

[38] Dominko, R., Li_2MSiO_4 (M = Fe and/or Mn) Cathode Materials. *Journal of Power Sources* **2008**, *184*, 462-468.

[39] Belharouak, I.; Abouimrane, A.; Amine, K., Evaluation of Li_2MnSiO_4 Cathode. Argonne National Laboratory, Presentation: March 20, 2009.

[40] Nytén, A.; Abouimrane, A.; Armand, M.; Gustafsson, T.; Thomas, J. O., Electrochemical Performance of Li_2FeSiO_4 as a New Li-Battery Cathode Material. *Electrochemistry Communications* **2005**, *7*, 156-160.

[41] Dominko, R.; Bele, M.; Gaberšček, M.; Meden, A.; Remškar, M.; Jamnik, J., Structure and Electrochemical Performance of Li_2MnSiO_4 and Li_2FeSiO_4 as Potential Li-battery Cathode Materials. *Electrochemistry Communications* **2006**, *8*, 217-222.

[42] Gong, Z. L.; Li, Y. X.; Yang, Y., Synthesis and Characterization of $Li_2Mn_xFe_{1-x}SiO_4$ as a Cathode Material for Lithium-Ion Batteries. *Electrochemical and Solid-State Letters* **2006**, *9 (12)*, A542-A544.

[43] Peng, C.-L.; Zhang, J.-F.; Cao, X.; Zhang, B., Synthesis of $Li_2Fe_{0.9}Mn_{0.1}SiO_4$/C Composites Using Glucose, as Carbon Source. *Journal of Central South University of Technology* **2010**, *17*, 504-508.

[44] Muraliganth, T.; Stroukoff, K. R.; Manthiram, A., Microwave-Solvothermal Synthesis of Nanostructured Li_2MSiO_4/C (M = Mn and Fe) Cathodes for Lithium-ion Batteries. *Chemistry of Materials* **2010**, *22 (20)*, 5754-5761.

[45] Zhang, S.; Deng, C.; Yang, S., Preparation of Nano-Li_2FeSiO_4 as Cathode Material for Lithium-Ion Batteries. *Electrochemical and Solid-State Letters* **2009**, *12 (7)*, A136-A139.

[46] Klein, L. C., Sol-Gel Processing of Silicates. *Annual Review of Materials Science* **1985**, *15*, 227-248.

[47] Fu, L. J.; Liu, H.; Li, C.; Wu, Y. P.; Rahm, E.; Holze, R.; Wu, H. Q., Electrode Materials for Lithium Secondary Batteries Prepared by Sol-Gel Methods. *Progress in Materials Science* **2005**, *50*, 881-928.

[48] Sakka, S.; Kamiya, K.; Makita, K.; Yamamoto, Y., Formulation of Sheets and Coating Films from Alkoxide Solutions. *Journal of Non-Crystalline Solids* **1984**, *63*, 223-235.

[49] Vogelsberger, W.; Opfermann, J.; Wank, U.; Schulze, H.; Rudakoff, G., On the Determination of Kinetic Parameters of Sol Formation, by Rheological Measurements. *Colloids and Surfaces A: Physiochemical and Engineering Aspects* **1993**, *78*, 99-108.

[50] Nakamura, T.; Tai, R.; Nishimura, T.; Tachibana, K., Spectroscopic Study on Metallorganic Chemical Vapor Deposition of Manganese Oxide Films. *Journal of The Electrochemical Society* **2005**, *152 (9)*, C584-C587.

[51] Jung, E.; Yoo, S. H.; Chung, T.-M.; Kim, C. G.; Kim, Y.; Jung, D. Y., Heterobimetallic Lithium Organogallium, Complexes: Potential Single Precursors for MOCVD of $LiMO_2$ Thin Films. *Inorganic Chemistry Communications* **2002**, *5*, 439-441.

[52] Phuong, N. M.; Neishi, K.; Sutou, Y.; Koike, J., Effects of Adsorbed Moisture in SiO_2 Substrates on the Formation of a Mn Oxide Layer by Chemical Vapor Deposition. *The Journal of Physical Chemistry C* **2011**, *115*, 16731-16736.

[53] Au, Y.; Lin, Y.; Kim, H.; Beh, E.; Liu, Y.; Gordon, R. G., Selective Chemical Vapor Deposition of Manganese Self-Aligned Capping Layer for Cu Interconnections in Microelectronics. *Journal of The Electrochemical Society* **2010**, *157 (6)*, D341-D345.

[54] Klaus, J. W.; Sneh, O.; George, S. M., Growth of SiO_2 at Room Temperature with the Use of Catalyzed Sequential Half-Reactions. *Science* **1997**, 1934-1936.